Time Domain Numerical Modelling of Graphene

Fatemeh Afshar

Department of Electrical & Computer Engineering

McGill University

Montréal, Canada

August 2018

A thesis submitted to McGill University in partial fulfillment of the requirements

of the degree of Doctor of Philosophy

Abstract

In this thesis, we focus on modelling a newly discovered material, called graphene, using time domain methods. First, a general finite-difference time-domain (FDTD) approach followed by FDTD update equations considering graphene is introduced. Subsequently, a new FDTD formulation for modelling intra-band conductivity term of graphene is proposed, in which graphene is modelled as a resistive sheet with a frequency-dependent conductivity. The formulation is first developed in the context of the vector wave finite-element time-domain (FETD) and then reduced to the FDTD based on the equivalence between these two techniques. The obtained formulation is easy-to-implement and does not alter the original FDTD update equations. It can be applied to an existing FDTD code by simply adding a correction term to appropriate variables.

In addition, an efficient method based on the recursive fast Fourier transform (FFT) to incorporate both the intra-band and inter-band conductivity terms of graphene into FDTD method is proposed. As it only requires numerical values of the conductivity, it not only does not enforce any restrictions on the conductivity models, but also can directly take into account material properties obtained from measurement. It reduces the total computational cost from $\boldsymbol{O(N^2)}$ to $\boldsymbol{O(Nlog^2N)}$ where $\boldsymbol{N}$ is the length of the unknown. The FDTD method is also modified and proven to retain the stability condition of the standard FDTD method.

Résumé

Cette thèse porte sur l'étude de la modélisation d'un matériau récemment découvert, appelé graphène, dans les méthodes du domaine temporal. Premièrement, une approche générale dans le domaine temporel à différences finies (FDTD) suivie par des équations de mise à jour FDTD prenant en compte le graphène est introduite. Par la suite, une nouvelle formulation FDTD pour la modélisation du terme de conductivité intra-bande du graphène est proposée, dans laquelle le graphène est modélisé comme une feuille résistive avec une conductivité dépendante de la fréquence. La formulation est d'abord développée dans le contexte du domaine temporel à éléments finis (FETD) de l'onde vectorielle puis réduite à la FDTD sur la base de l'équivalence entre ces deux techniques. La formulation obtenue est facile à mettre en œuvre et ne modifie pas les équations originales de mise à jour FDTD. Elle peut être appliquée à un code FDTD existant en ajoutant simplement un terme de correction aux variables appropriées.

De plus, une méthode efficace basée sur la transformée de Fourier rapide (FFT) récursive pour incorporer à la fois les termes de conductivité intra-bande et inter-bande du graphène dans la méthode FDTD est proposée. Comme elle ne nécessite que des valeurs numériques de la conductivité, non seulement elle n'applique aucune restriction sur les modèles de conductivité, mais elle peut également prendre directement en compte les propriétés matérielles obtenues à partir de la mesure. Il réduit le coût de calcul total de $\boldsymbol{O(N^2)}$ à $\boldsymbol{O(Nlog^2N)}$ où $\boldsymbol{N}$ est la longueur de l'inconnu. La méthode FDTD est également modifiée et prouvée pour conserver la condition de stabilité de la méthode FDTD standard.

Acknowledgments

I would like to express my deepest gratitude to my supervisor Prof. Dennis D. Giannacopoulos for his continued support, encouragement and patience during my long Ph.D. study.

I also would like to extend my appreciation to Dr. Ali Akbarzadeh Sharbaaf, without whom none of my work would have been possible. He was my mentor, my unofficial co-supervisor and most importantly a dear friend who helped me wholeheartedly with all his knowledge and experience.

And last but not least, I am greatly indebted to my dear husband Dr. Soroush Nazarpour for his unconditional and continuous love and support.

Research Publications

F. Afshar, A. Akbarzadeh-Sharbaf, and D. Giannacopoulos. "A Provably Stable and Simple FDTD Formulation for Electromagnetic Modeling of Graphene Sheets." IEEE Trans. Magn., vol. 52, no. 3, pp. 379–382, March. 2016.

F. Afshar, A. Akbarzadeh-Sharbaf, D. D. Giannacopoulos, and S. McFee, "Wideband Finite-Difference Time-Domain Modeling of Graphene via Recursive Fast Fourier Transform," Progress In Electromagnetics Research C, Vol. 75, 139-145, 2017.

F. Afshar, A. Akbarzadeh-Sharbaf, D. D. Giannacopoulos, and S. McFee, " Wideband Finite-Difference Time-Domain Modeling of Graphene via Recursive Fast Fourier Transform," IEEE Conference on Electromagnetic Field Computation (CEFC 2016), Miami, FL, USA.

F. Afshar, A. Akbarzadeh-Sharbaf, and D. D. Giannacopoulos. A Provably Stable and Simple FDTD Formulation for Electromagnetic Modeling of Graphene Sheets. 20th International Conference on the Computation of Electromagnetic Fields (Compumag 2015), Montreal, Canada.

Contents

List of Figures

List of Acronyms

CVD	Chemical Vapour Deposition
CNT	Carbon Nano Tube
GNR	Graphene NanoRibbon
SPP	Surface Plasmon Polariton
EMI	ElectroMagnetic Interference
EM	ElectroMagnetic Field
FDTD	Finite Difference Time Domain
SBC	Surface Boundary Condition
ADE	Auxiliary Differential Equation
E	Electric Field
H	Magnetic Field
FETD	Finite element Time Domain
TDFEM	Time Domain Finite Element Method
ODE	Ordinary Differential Equation
CN	Crank-Nicolson
ADI	Alternating Direction Implicit
DOF	Degree Of Freedom
PML	Perfectly Matched Layer
PEC	Perfect Electric Conductor
TD	Time Domain
VWE	Vector Wave Equation
RC	Recursive Convolution
CFL	Courant-Friedriche-Lewy
MEMS	Micro-ElectroMechanical Systems

Chapter 1

Introduction

1.1 Motivation

It all started in 2010, when Nobel prize in Physics was given to Andre Geim and Konstantin Novoselov, two professors at the University of Manchester for the discovery of graphene. They isolated graphene through a repetitive peeling-unpeeling of a crystalline flake graphite with scotch tape. Even though the process looks orthodox, it was the first successful effort to exfoliate graphite into single-layer of graphene. One may think this was just a lucky draw. We believe otherwise. They were both aware of the prior research done on the electrical properties of very thin graphite such as the work of Fujibayashi published at 1972 in Journal of Physical Society of Japan. It was their insight that enabled them to follow the trend of discoveries where thinning graphite to single layer should reveal outstanding properties and they just did it. What we learned from the story was neither the simplicity of a discovery by scotch tape nor the shiny Nobel prize, but it was the importance of having an insight before acting.

Today many researchers around the world are continuing the research of Geim and Novoselov and developing applications of graphene. This thesis was motivated by the need to develop a technique to model graphene interaction with electromagnetic fields in order to assist the researchers prior to conducting the experiment. In other words, the goal of this thesis is to bring

the insight to their research to help them to see more possibilities this magical material can bring into our world.

1.2 Graphene Overview

The past decade has witnessed the discovery of a new 2D nanomaterial called graphene, which possesses unique properties suited to various applications. After winning the Nobel prize by its discoverers, it attracted tremendous attention in fields ranging from material science, nanotechnology to physics and electrical engineering. Scientists across the globe have made many discoveries on graphene's material properties and potential applications. In the following section, an overview of graphene properties and its potential applications are provided. Moreover, different modelling techniques used for graphene will be mentioned.

1.2.1 Graphene: The Material of 21st Century

In 2004, University of Manchester researchers Andre Geim and Kostantin Novoselov discovered graphene - a nanomaterial possessing truly extraordinary properties. In 2010, Geim and Novoselov were awarded the Nobel prize in Physics for their discovery of this "wonder material," which comprises a single layer of carbon atoms arranged in a honeycomb lattice with only 1 molecule thickness (hence its 2D classification) [1]. The method that accidently led to the discovery of graphene is called the "scotch tape" method. An adhesive tape is used for the exfoliation of graphite down to the single layer of graphene. The procedure involves repeated pealing of few-layers of graphene from flakes of graphite (Fig 1.1-1.3).

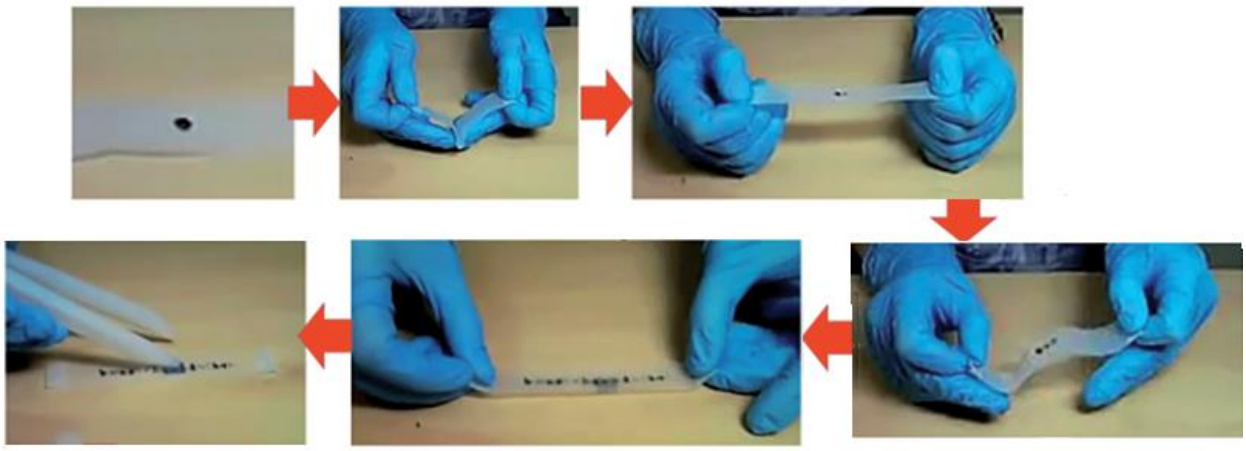

Fig. 1.1. Mechanical cleavage of graphene from graphite using adhesive tape [2].

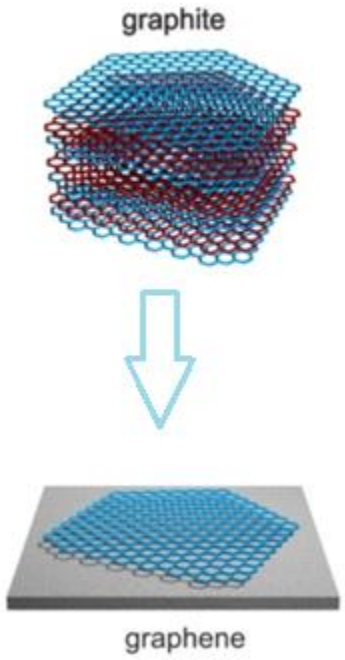

Fig. 1.2. Graphene as one single layer of graphite [2].

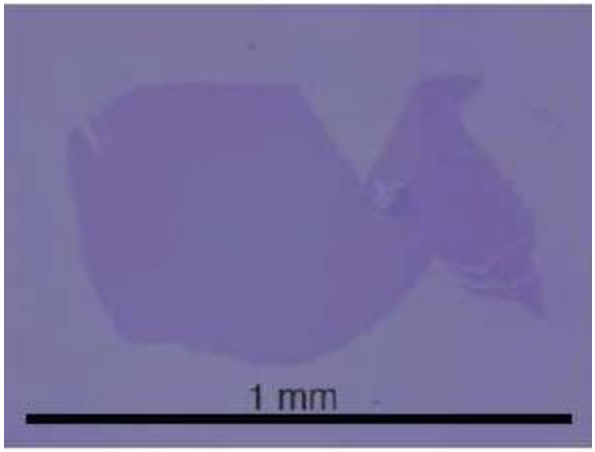

Fig. 1.3. A graphene sample at the millimeter scale [2].

Graphene is the thinnest material known to mankind, with an exceptionally high theoretical surface area (2630 m^2 per gram). Atomically, it is the strongest material ever measured, is extremely elastic (stretchable), and has exceptional thermal and electrical conductivity, making it the substance a design engineer's dreams [2]. Among all these characteristics, the one that is mostly interesting in its electrical properties that include its high carrier mobility, measured in various devices as 8000-10000 $cm^2v^{-1}s^{-1}$ and could reach 200000 $cm^2v^{-1}s^{-1}$ in suspended graphene [3]. On the other hand, graphene's non-electronic properties bring a new dimension to graphene research. A defect-free sheet of graphene was found to have a record-breaking strength of 42 Nm^{-1}, reaching the theoretical limit, as well as a Young's modulus of 1.0 TPa, which is also a record value [4]. The one-atom-thick graphene is also found to be impermeable to gases, which could be of interest in bio-molecular and ion transport research [5].

The technology of manufacturing graphene has advanced in the past few years and both the size and quality of the graphene made have been significantly improved. The experimental discovery of graphene shows that while 2-D crystals do not grow naturally, they can be made artificially by

two general approaches. One starts from graphite (top-down approach), the other one from small molecules that are used to build up graphene (bottom-up approach).

As mentioned above, transforming graphite to graphene can be performed mechanically using adhesive tape [6], mechanically in solvents by sonication [7], shear mixing or ball milling [8]. In addition, the delamination of single layers of graphite can be facilitated using chemical methods that involve chemical functionalization and de-functionalization after processing. The latter approach to graphene aims on the synthesis of graphene on solids using a carbon source. The method of choice is most often chemical vapor deposition (CVD) [9] using a metal surface and small molecules, such as methane or acetylene.

Each of these approaches have their own challenges that must be overcome in the future to obtain high performance materials utilizing the unique properties of graphene, such as the high mobility of charge carriers, mechanical strength, conductivity and transparency combined with flexibility [2]. The aforementioned graphene properties and current level of manufacturing capability make graphene a good candidate for many novel devices as will be introduced in the next section.

1.2.2 Graphene Applications

Understandably, graphene-related patent filings have risen significantly around the world over the past several years. The UK is currently a hotbed of activity in graphene, with the University of Manchester acting as a magnet for millions of dollars of research funding. Entrepreneurial and investment activities associated with graphene have increased significantly. Patenting graphene-based applications has also increased by major electronic industries like Technology stalwarts Samsung and IBM. Today, the range of potential applications for graphene is limited only by one's imagination [2].

Electronics is the field where graphene is expected to have an important impact. Due to its outstanding electronic properties, graphene is a material of choice for devices working at radio frequencies [10]. Furthermore, its transparency and advantageous mechanical properties make it a suitable candidate to replace elements of electronic devices, such as touch screens and displays (Fig. 1.4). It is a promising candidate to replace traditional transparent conducting films, such as Tin-doped Indium Oxide (ITO) or Aluminum-doped Zinc-Oxide (AZO), which are expensive, less efficient and toxic [11].

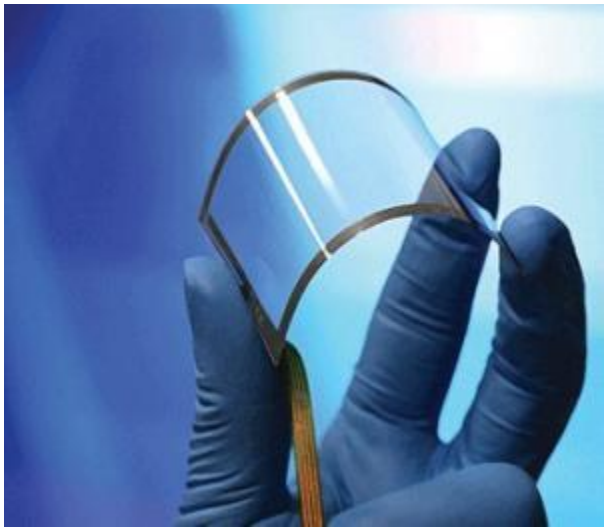

Fig. 1.4. South Korean researchers made a foldable touch screen from a 30-inch piece of graphene. (Photo courtesy of Prof. Byung Hee Hong)

Graphene has been also intensively studied as a base material for energy harvesting. Graphene could enhance the efficiency and integration of solar cells, acting as a transparent electrode [12-13].

Moreover, graphene-based Micro-ElectroMechanical Systems (MEMS) devices and transistors, e.g., Field Effect Transistors (FET), have developed rapidly and are now considered an option for post-silicon electronics [14].

Another application worth mentioning is graphene nano-antennas. Earlier research on nano-antennas was focusing on the carbon nanotube (CNT) based antennas. CNTs support slow-wave propagation, whereby the phase velocity of electromagnetic waves propagating in CNT is on the order of $c_0/100$ to $c_0/50$ (c_0 being the speed of light in a vaccum) [15]. Despite their help in miniaturization of structures, they suffer from a major drawback which is its high resistance due to its extremely high aspect ratio (length/cross sectional area). As a result of the high resistance, the CNT nano-antenna often has a low efficiency. Fig. 1.5 shows a CNT antenna and a graphene nanoribbon (GNR) antenna.

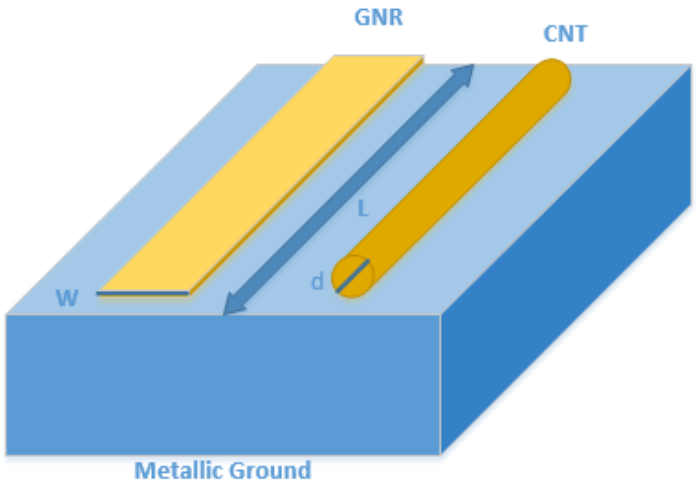

Fig. 1.5. CNT nano-patch antenna on the right and Graphene nano-patch antenna on the left [2].

Another attribute of graphene which supports surface plasmon polariton (SPP) wave have recently caught scientists' attention [16-17]. SPPs are infrared or visible-frequency electromagnetic excitations at the interface between a metal and a dielectric material.

The unique properties of SPPs provide pathways to harnessing light in ways not possible with conventional optics, resulting into novel applications such as super resolution imaging, SPP lithography, SPP-assisted absorption, SPP-based antennas and devices.

Recently Vakil and Engheta [17] discussed a new device in which the SPP properties of highly doped graphene play a key role. Replacing metals such as gold or silver with graphene in SPP-related device is advantageous since the material properties of graphene are tunable via external electric or magnetic fields, and it supports SPPs with longer propagation lengths. In this case, graphene behaves like a thin metal layers where its conductivity is a function of its chemical potential (which will be discussed in the next section). Chemical potential is dependent upon gate voltage and/or chemical doping. Hence, graphene conductivity is adjustable with chemical doping. Graphene's tunable conductivity allows it to tailor electromagnetic fields into desired spatial patterns with longer propagation lengths making graphene a promising alternative to metal-based plasmonics [16] with SPPs that are tightly confined on the surface.

Fig. 1.6(a) reveals the possibility of having a selected part of the graphene sheet to support SPP waves while not on the other part, and this is done by varying the sign of the imaginary part of the conductivity via applying different gate voltages. The damping loss of its SPPs is relatively low; hence, the propagation length could reach dozens of wavelengths of SPPs. The tuning can be done in real time by varying the gate voltage, and it can be done inhomogeneously to form a conductivity pattern on a single graphene sheet [17]. Fig. 1.6(b) shows alternatively, an uneven ground plane underneath the graphene can be implemented to design the conductivity profile on the graphene. With the above-mentioned techniques, transformation optical devices, such as graphene-based Luneburg lens, can be designed.

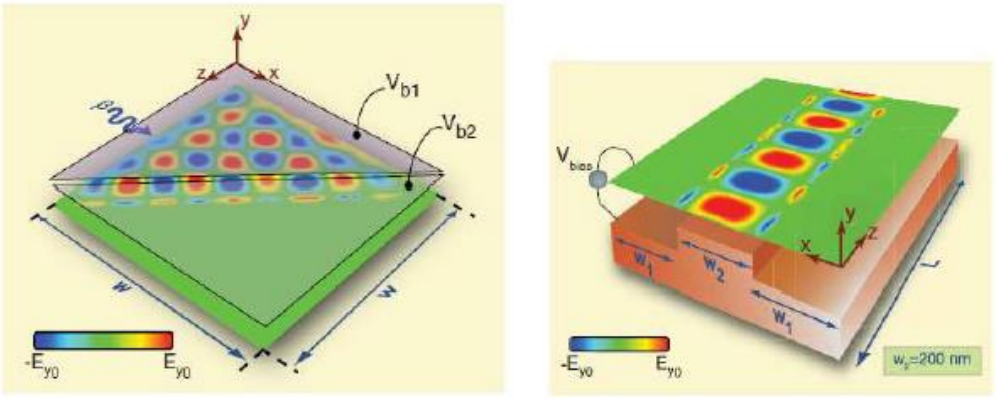

Fig. 1.6: (a) Graphene conductivity controlled by bias voltages [17]. (b) Graphene conductivity controlled by uneven ground plane [17].

Graphene-based thermoplastic/thermoset composites have attracted significant attention as EMI shielding materials due to the low percolation threshold in mechanical and the electrical properties of the graphene filled composites. It is very essential to protect interference prone equipment from being malfunction. Thus, metal and metallic composites were the choice for shielding purpose due to their high electrical conductivity. However, difficulty in processing, heavy weight, and its chemical instability have urged scientists to look beyond it. Therefore, graphene filled polymer composites have started getting attention as EMI shielding materials due to their light weight, large specific surface area and good electrical conductivity [2].

The above-mentioned examples are just a few of many applications being researched with graphene. Typically finding the electromagnetic fields in these subwavelength geometries requires numerical approaches to solve Maxwell's equations. Below, we describe different numerical methods used so far to model graphene**.**

1.2.3 Different Numerical Methods to Simulate Graphene Devices

In recent years, with the introduction of graphene-based applications, such as waveguides, nano-antennas, or electromagnetic (EM)-shielding; the need for studying their EM behavior has emerged. In a macroscopic EM fields context, graphene behaves as a surface with conductivity that depends on chemical doping or external field bias [18]. In order to study the scattering, radiation and wave-guiding properties of graphene, Maxwell's equations need to be solved either in two-dimensional or three-dimensional space. Since obtaining the analytic solution of Maxwell's equations in most cases is impossible, the use of numerical simulation methods is helpful.

Graphene has been modeled in various kinds of numerical methods, both in the frequency and time domains, such as the method of moment (MoM) [19], the finite-element method (FEM) [20], and the finite-difference-time-domain (FDTD) method [21]– [25].

In 2011 Vakil and Engheta [17] proposed a frequency domain method considering graphene sheet as a thin layer with a volumetric conductivity. They conducted the simulations at a particular frequency, where the graphene conductivity value (at that desired frequency) is directly entered to a commercial software tools such as CST Studio Suite [26] and COMSOL Multiphysics [27]. However, to study the transient behaviour of the device and obtain the result for a wide frequency band with a single simulation in time, numerical methods in time-domain have huge advantages over frequency-domain methods.

The FDTD method is arguably the simplest, both conceptually and in terms of implementation, numerical technique for solving Maxwell's equations [28]- [29] and it is straightforward to incorporate the macroscopic model into the general FDTD scheme to solve problems in electromagnetics. Modeling graphene in FDTD can be performed in different ways with dramatic variation in the efficiency and resource requirements of the simulation. Up to now, three

approaches have been used to model the graphene in FDTD methods which are: 1) regular FDTD method with very fine field discretization in the graphene layer [21]- [22]; 2) the sub-cell FDTD approach [23]; and 3) the graphene as a surface boundary condition (SBC) in FDTD [24]. Since graphene is very thin (one atomic thick layer) and because of the linear relationship (introduced by Yee [30]) between the discretization steps in space and time, finer spatial grid needs finer time steps, the first approach requires a significant amount of memory and time which makes it a poor option in practice. In spite of the merits of the last two approaches, they share at least two major drawbacks: first, they require different update equations in the vicinity of the graphene sheet and a special type of perfectly-matched layer (PML) [31] which makes the programming difficult; and second, the effect of the modified equations on the stability of the underlying FDTD has not been analytically studied.

Early SBC works in the FDTD method, introduced in 1992 by Maloney and Beggs, such as the surface impedance boundary condition approach considered only the reflection from a layer [32]-[33]. Later that year, Wu and Han [34] came up with a method for implementation of a resistive sheet boundary condition which calculated both transmission and reflection through an infinitesimal thin sheet, but the method suffered from instability [34-36]. The previous methods impose a restriction on the conductivity of the resistive thin sheets which are not applicable for modelling graphene as an SBC in the FDTD method.

1.3 Thesis Outline and Contributions

The outline and the highlights of the contributions of this thesis are as follows:

Chapter 2 is dedicated to the study of the FDTD modeling of graphene. First, the graphene conductivity model is introduced, and the FDTD update equations for graphene are developed. Then the Von Neumann stability analysis for intra-band conductivity has been performed and by taking into account that all eigenvalues of the system should reside on or inside the unit circle in order for our system to be stable, we obtain the criteria for time step size.

Chapter 3 first introduces FETD formulation and hybrid FDTD-FETD method for developing an efficient technique with better stability to solve electromagnetic problems for graphene. Moreover, some efforts have been made to improve the stability criteria arising in the FDTD solution, which is often more severe and limiting in dispersive cases. In the following sections, some important aspects of the FETD and FDTD formulations are discussed and reviewed.

Chapter 4 establishes new FDTD formulation for modelling graphene, in which graphene is modelled as a resistive sheet with a frequency-dependent conductivity. The formulation is first developed in the context of the vector wave finite-element time-domain (FETD) and then reduced to the FDTD based on the equivalence between these two techniques. The obtained formulation is easy-to-implement and does not alter the original FDTD update equations. It can be applied to an existing FDTD code by simply adding a correction term to appropriate variables. One of the main contributions of our work in this chapter is analyzing the stability of the proposed formulation, which has not been done previously. Accuracy and stability of the new formulations have been studied through some numerical examples.

Chapter 5 includes the inter-band conductivity of graphene which is a logarithmic term and not easy to model. A new method based on the recursive fast Fourier transform (FFT) to incorporate both conductivity terms of graphene into FDTD method is proposed. As it only requires numerical values of the conductivity, it not only does not enforce any restrictions on the conductivity models, but can also directly take into account material properties obtained from measurement. It reduces the total computational cost from $\boldsymbol{O}(\boldsymbol{N^2})$ to $\boldsymbol{O}(\boldsymbol{Nlog^2N})$ where $\boldsymbol{N}$ is the length of the unknown. The FDTD method is also modified and proven to retain the stability condition of the standard FDTD method.

Chapter 6 concludes this thesis with a summary of work done and contributions, along with possible future work related to this thesis.

The co-authors of my publications contributed as advisory members to develop the theoretical formalism, perform the analytical verifications and simulations, and edit the manuscripts.

Chapter 2

Finite-difference-Time-Domain Modelling of Graphene

2.1 Introduction

In this chapter, we introduce the macroscopic frequency-dependent graphene conductivity model and then we touch upon general FDTD equations followed by FDTD update equations for graphene. In the last part, the stability analysis for the update scheme is provided.

2.2 Graphene Conductivity Model

Graphene has a frequency-dependent complex-valued conductivity. The macroscopic graphene conductivity model used in the FDTD method consists of two terms: 1) inter-band conductivity and 2) intra-band conductivity. The graphene surface conductivity (in units of [S]) is given by the Kubo formula in an integral form [37] as shown in equation (2.1).

$$\sigma(\omega,\mu_c,\gamma,T) = \frac{je^2(\omega-2j\gamma)}{\pi\hbar^2}\left[\frac{1}{(\omega-2j\gamma)^2}\int_0^\infty \epsilon\left(\frac{\partial f_d(\epsilon)}{\partial\epsilon}-\frac{\partial f_d(-\epsilon)}{\partial\epsilon}\right)d\epsilon\right.$$
$$\left.-\int_0^\infty \frac{f_d(-\epsilon)-f_d(\epsilon)}{(\omega-2j\gamma)^2-4(\epsilon/\hbar)^2}d\epsilon\right]. \qquad (2.1)$$

In this equation, $f_d(\epsilon) = \left(e^{(\epsilon-\mu)/K_BT}+1\right)^{-1}$ is the Fermi-Dirac distribution, ω is the angular frequency in rad/s, and γ is the scattering rate in s^{-1}. In addition, μ_c is the chemical potential in

eV, which can be controlled by chemical doping or by applying a bias voltage, T is the temperature in Kelvin, e is the electron charge, $\hbar$ is the reduced Planck's constant, and k_B is the Boltzmann constant. The first term showcases the intra-band carrier relaxation contribution, and the second term is from the inter-band transition contribution.

The equation (2.1) in its integral form cannot be integrated in the FDTD scheme and needs to be simplified [37]. Therefore, intra-band conductivity can be evaluated as:

$$\sigma_{intra}(\omega, \mu_c, \gamma, T) = \frac{je^2 k_B T}{(\omega - j2\gamma)\pi\hbar^2}\left(\frac{\mu_c}{k_B T} + 2ln\left(exp^{(-\mu_c/k_B T)} + 1\right)\right) \qquad (2.2)$$

and the inter-band conductivity can be approximated by:

$$\sigma_{inter}(\omega, \mu_c, \gamma) = -j\frac{e^2}{4\pi\hbar}\ln\left(\frac{2|\mu_c| - (\omega - j2\gamma)\hbar}{2|\mu_c| + (\omega - j2\gamma)\hbar}\right) \qquad (2.3)$$

Fig. 2.1 demonstrates the real and imaginary parts of graphene conductivity with two different chemical potential μ_c values.

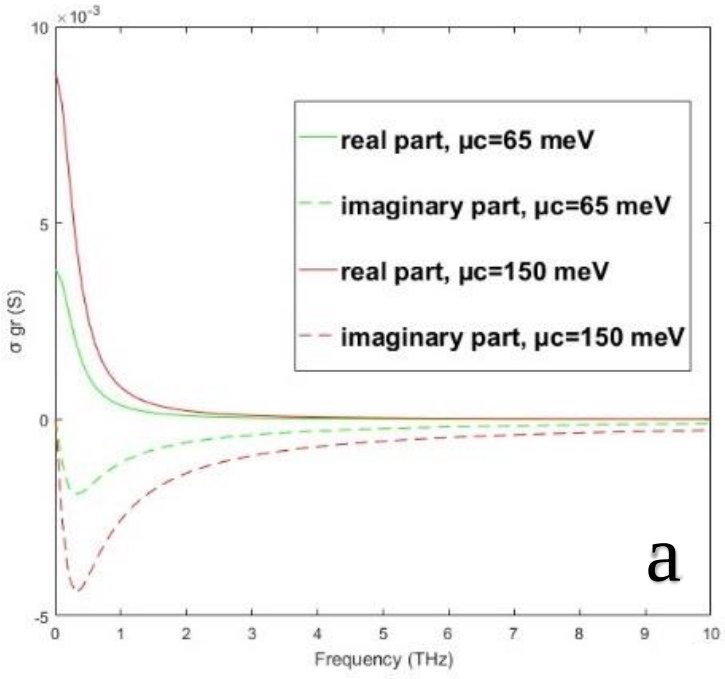

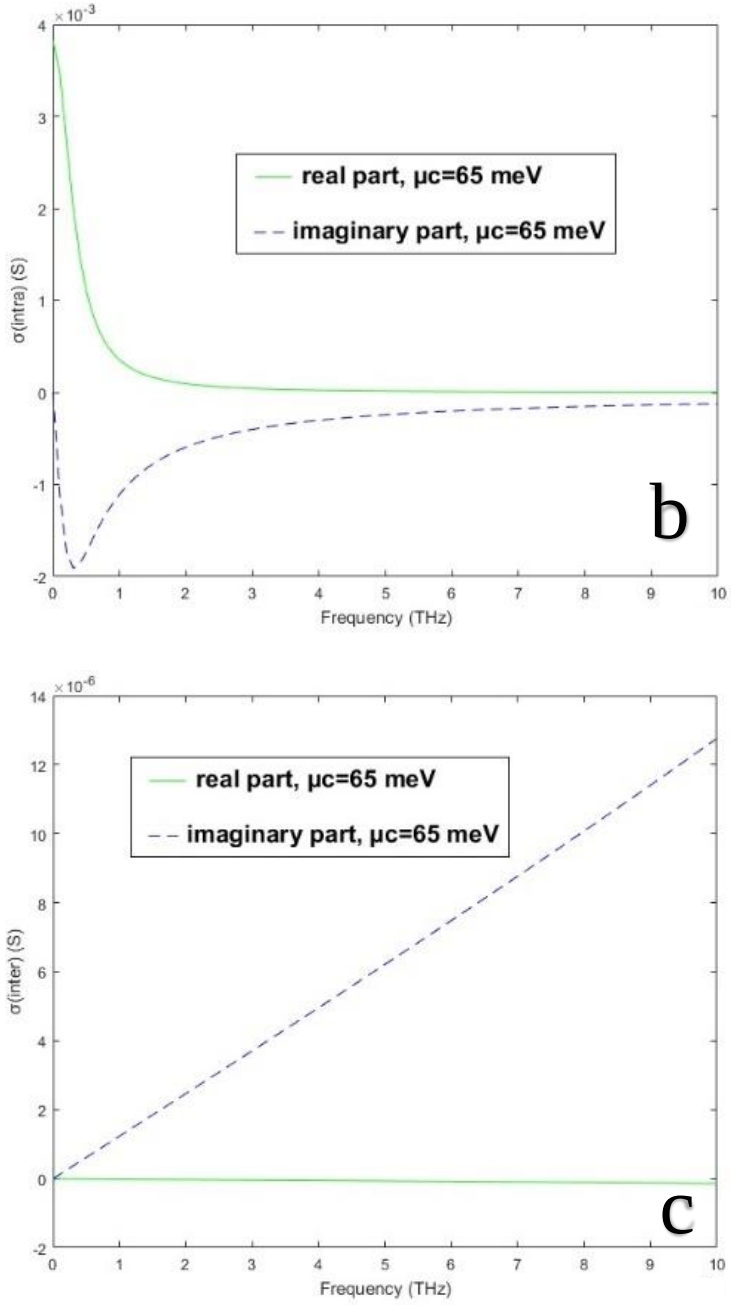

Fig. 2.1. a) Plot of the real and imaginary part of the graphene conductivity calculated using equation (2.1) for $\mu_c = 65\ meV$ and $\mu_c = 150\ meV$ at T = 30 K and $\gamma = 10^{12}$, b) Plot of the real and imaginary part of the intra-band conductivity term for $\mu_c = 65\ meV$, c) Plot of the real and imaginary part of the inter-band conductivity term for $\mu_c = 65\ meV$.

When the permittivity or permeability of a material are functions of frequency, the material is dispersive. In the frequency domain, the relationship between the electric field and current density for isotropic materials is given by $\vec{J}(\omega) = \sigma(\omega)\vec{E}(\omega)$. Since FDTD solves Maxwell's equations in the time domain, incorporating the dispersive property of the material requires additional numerical effort. One of the approaches to alleviate this problem is to use auxiliary differential equations (ADE) [38-39] to model the dispersive material properties in the time domain. The ADE method requires that the dispersive conductivity be represented as a ratio of polynomials in ω, i.e. the Drude model. The intra-band conductivity can be expressed by a Drude-like expression [40]:

$$\sigma_{intra}(\omega, \mu_c, \gamma, T) = \frac{\alpha}{\omega - j2\gamma} \tag{2.4}$$

In which $\alpha = \frac{je^2 k_B T}{\pi\hbar^2}\left(\frac{\mu_c}{k_B T} + 2ln\left(e^{(-\mu_c/k_B T)} + 1\right)\right)$. This expression can be directly implemented in the FDTD formulation; however, due to the complexity of the inter-band term, it cannot be directly converted into a discrete-time relation using the ADE method.

George W. Hanson in 2013 [18] showed that for the frequency $\omega \ll 2\mu_c/\hbar$, the inter-band term is negligible and the intra-band term is dominant. Considering $\mu_c > 0.05$, which is a practical condition, the intra-band is the dominant term in gigahertz and low terahertz regimes, resulting in the fact that many scientists working in the microwave regime neglect this term for the straightforward implementation of the conductivity in FDTD scheme. However, the inter-band conductivity must be included when considering higher frequencies and optical behavior with optical energies near the chemical potential.

2.3 Finite-Difference Time-Domain Method

The finite-difference time-domain (FDTD) method is a numerical method to solve partial differential equations such as Maxwell's equations in the time domain. It was introduced by Yee in 1966 [30] and further developed by Taflove in the 1970's [39]. The method can be applied to EM problems with different boundary shapes, different kinds of boundary conditions, and regions containing a number of different materials. The application of FDTD is simple and straightforward as it involves only simple arithmetic in the derivation of discretized equations and in writing the corresponding computer codes. Since it is a time-domain method, one single run of simulation can provide information over a large bandwidth when the excitation is chosen to be of large bandwidth.

In linear, lossless and isotropic medium the differential form of Maxwell's equations, Faraday's Law (equation (2.5)) and Ampere's Law (equation (2.6)) are solved to update the electric fields ($\vec{E}$) and magnetic fields ($\vec{H}$) in space and time.

$$\nabla \times \vec{E} = -\mu \frac{\partial \vec{H}}{\partial t} - \vec{M}. \qquad (2.5)$$

$$\nabla \times \vec{H} = \varepsilon \frac{\partial E}{\partial t} + \vec{J}. \qquad (2.6)$$

where ε (F/m) and μ (H/m) are electrical permittivity and magnetic permeability, respectively. Assuming $\vec{J} = 0$ and $\vec{M} = 0$, the two Maxwell's curl equations (2.5), (2.6) can be written as six scalar equations in Cartesian coordinates. Electric field can be written as:

$$\frac{\partial E_x}{\partial t} = \frac{1}{\varepsilon}\left[\frac{\partial H_z}{\partial y} - \frac{\partial H_y}{\partial z}\right] \qquad (2.7a)$$

$$\frac{\partial E_y}{\partial t} = \frac{1}{\varepsilon}\left[\frac{\partial H_x}{\partial z} - \frac{\partial H_z}{\partial x}\right] \qquad (2.7b)$$

$$\frac{\partial E_z}{\partial t} = \frac{1}{\varepsilon}\left[\frac{\partial H_y}{\partial x} - \frac{\partial H_x}{\partial y}\right] \qquad (2.7c)$$

and for magnetic field, we will have:

$$\frac{\partial H_x}{\partial t} = \frac{1}{\mu}\left[\frac{\partial E_y}{\partial z} - \frac{\partial E_z}{\partial y}\right] \qquad (2.8a)$$

$$\frac{\partial H_y}{\partial t} = \frac{1}{\mu}\left[\frac{\partial E_z}{\partial x} - \frac{\partial E_x}{\partial z}\right] \qquad (2.8b)$$

$$\frac{\partial H_z}{\partial t} = \frac{1}{\mu}\left[\frac{\partial E_x}{\partial y} - \frac{\partial E_y}{\partial x}\right] \qquad (2.8c)$$

As shown in Fig. 2.2, the Yee's cell of dimension $\Delta x \times \Delta y \times \Delta z$ is introduced as a unit cell of the discretized spatial domain and Δt as temporal increment steps. Any function of space and time can be written as: $u(i\Delta x, j\Delta y, k\Delta z, n\Delta t)$.

This method is an explicit finite difference method using central difference for space and time on a staggered Cartesian grid (leap-frog method) and it is second order accurate.

$$\frac{\partial u^n(i,j,k)}{\partial x} = \frac{\partial u^n(i+1/2,j,k) - \partial u^n(i-1/2,j,k)}{\Delta x} + O(\Delta x^2) \qquad (2.9)$$

$$\frac{\partial u^n(i,j,k)}{\partial t} = \frac{\partial u^{n+1}(i,j,k) - \partial u^n(i,j,k)}{\Delta t} + O(\Delta t^2) \qquad (2.10)$$

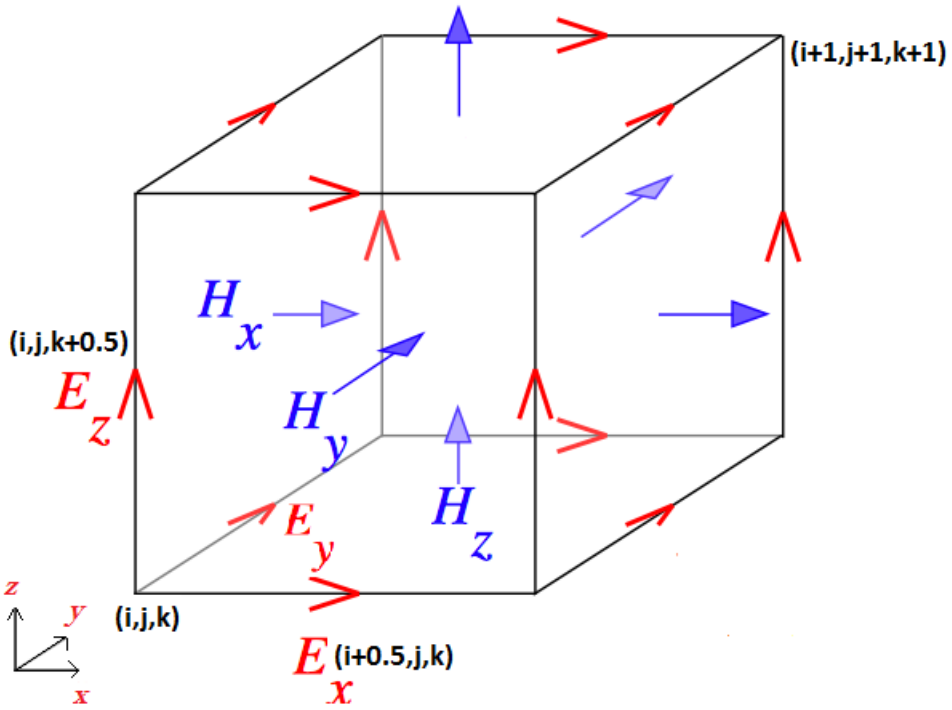

Fig 2.2. Position of electric and magnetic field vector components in a unit Yee cell [30].

All fields are initially set to zero in the simulation domain. With a source excitation, all E fields are updated at the integer time step n and H fields are updated at half time steps $n + 1/2$ using the E values at time step n. Repeating this process allows the simulation to march in time.

2.3.1 The Leap Frog Scheme

Considering the discretization method in equations (2.9) and (2.10), FDTD update equations in homogeneous materials with $\sigma = 0$ for the electromagnetic field components with the exact locations shown in Fig 2.2 are as follows:

$$E^{n+1}_{x,(i+\frac{1}{2},j,k)} = E^{n}_{x,(i+\frac{1}{2},j,k)} + \frac{\Delta t}{\varepsilon}\left[\frac{H^{n+\frac{1}{2}}_{z,(i+\frac{1}{2},j+\frac{1}{2},k)} - H^{n+\frac{1}{2}}_{z,(i+\frac{1}{2},j-\frac{1}{2},k)}}{\Delta y} - \frac{H^{n+\frac{1}{2}}_{y,(i+\frac{1}{2},j,k+\frac{1}{2})} - H^{n+\frac{1}{2}}_{y,(i+\frac{1}{2},j,k-\frac{1}{2})}}{\Delta z}\right] \quad (2.11a)$$

$$E^{n+1}_{y,(i,j+\frac{1}{2},k)} = E^{n}_{y,(i,j+\frac{1}{2},k)} + \frac{\Delta t}{\varepsilon}\left[\frac{H^{n+\frac{1}{2}}_{x,(i,j+\frac{1}{2},k+\frac{1}{2})} - H^{n+\frac{1}{2}}_{x,(i,j+\frac{1}{2},k-\frac{1}{2})}}{\Delta z} - \frac{H^{n+\frac{1}{2}}_{z,(i+\frac{1}{2},j+\frac{1}{2},k)} - H^{n+\frac{1}{2}}_{z,(i-\frac{1}{2},j+\frac{1}{2},k)}}{\Delta x}\right] \quad (2.11b)$$

$$E^{n+1}_{z,(i,j,k+\frac{1}{2})} = E^{n+1}_{z,(i,j,k+\frac{1}{2})} + \frac{\Delta t}{\varepsilon}\left[\frac{H^{n+\frac{1}{2}}_{y,(i+\frac{1}{2},j,k+\frac{1}{2})} - H^{n+\frac{1}{2}}_{y,(i-\frac{1}{2},j,k+\frac{1}{2})}}{\Delta x} - \frac{H^{n+\frac{1}{2}}_{x,(i,j+\frac{1}{2},k+\frac{1}{2})} - H^{n+\frac{1}{2}}_{x,(i,j-\frac{1}{2},k+\frac{1}{2})}}{\Delta y}\right] \quad (2.11c)$$

$$H^{n+\frac{1}{2}}_{x,(i,j+\frac{1}{2},k+\frac{1}{2})} = H^{n-\frac{1}{2}}_{x,(i,j+\frac{1}{2},k+\frac{1}{2})} - \frac{\Delta t}{\mu}\left[\frac{E^{n}_{z,(i,j+1,k+\frac{1}{2})} - E^{n}_{z,(i,j,k+\frac{1}{2})}}{\Delta y} - \frac{E^{n}_{y,(i,j+\frac{1}{2},k+1)} - E^{n}_{y,(i,j+\frac{1}{2},k)}}{\Delta z}\right] \quad (2.12a)$$

$$H^{n+\frac{1}{2}}_{y,(i+\frac{1}{2},j,k+\frac{1}{2})} = H^{n-\frac{1}{2}}_{y,(i+\frac{1}{2},j,k+\frac{1}{2})} - \frac{\Delta t}{\mu}\left[\frac{E^{n}_{x,(i+\frac{1}{2},j,k+1)} - E^{n}_{x,(i+\frac{1}{2},j,k)}}{\Delta z} - \frac{E^{n}_{z,(i+1,j,k+\frac{1}{2})} - E^{n}_{z,(i,j,k+\frac{1}{2})}}{\Delta x}\right] \quad (2.12b)$$

$$H^{n+\frac{1}{2}}_{z,(i+\frac{1}{2},j+\frac{1}{2},k)} = H^{n-\frac{1}{2}}_{z,(i+\frac{1}{2},j+\frac{1}{2},k)} - \frac{\Delta t}{\mu}\left[\frac{E^{n}_{y,(i+1,j+\frac{1}{2},k)} - E^{n}_{y,(i,j+\frac{1}{2},k)}}{\Delta x} - \frac{E^{n}_{x,(i+\frac{1}{2},j+1,k)} - E^{n}_{x,(i+\frac{1}{2},j,k)}}{\Delta y}\right] \quad (2.12c)$$

2.4 Implementing Graphene in FDTD method at Microwave Frequencies

To incorporate graphene, J in equation (2.6) will not be zero. By using just intra-band conductivity, and approximating it with Drude-like formula equation (2.4), the conduction current J can be updated as:

$$\vec{J}(\omega) = \sigma(\omega).\vec{E}(\omega) = \frac{\sigma_0}{1 + j\omega\tau}\vec{E}(\omega) \qquad (2.13)$$

where, $\sigma_0 = j\tau\alpha$.

$$\vec{J}(\omega) + j\omega\tau\vec{J}(\omega) = \sigma_0\vec{E}(\omega) \qquad (2.14)$$

which in time domain it becomes:

$$\vec{J}(t) + \tau\frac{\partial\vec{J}(t)}{\partial t} = \sigma_0\vec{E}(t) \qquad (2.15)$$

Using the leap-frog method to obtain the discrete form of $\frac{\partial\vec{J}(t)}{\partial t}$ in time and taking the average value of $\vec{J}(t)$ and $\vec{E}(t)$ results in the following equations:

$$\frac{J^{n+1} + J^n}{2} + \tau\frac{J^{n+1} - J^n}{\Delta t} = \sigma_0\frac{E^{n+1} + E^n}{2} \qquad (2.16)$$

$$J^{n+1} = \alpha J^n + \beta(E^{n+1} + E^n) \qquad (2.17)$$

where, $\alpha = \frac{(2\tau - \Delta t)}{(2\tau + \Delta t)}$, and $\beta = \frac{\sigma_0\Delta t}{(2\tau + \Delta t)}$.

In order to obtain J^{n+1}, we need to have E^{n+1} from the same step. By discretizing (2.5) and (2.6) in space and considering $\delta\{\cdot\}$ as the discrete curl operator, we will have the discrete form of

the fields in space. Again, by using the leap-frog method to obtain the discrete form in time and finally by taking the average value of J, we will have:

$$E^{n+1} = E^n - \frac{\Delta t}{\varepsilon}\delta\left\{H^{n+\frac{1}{2}}\right\} - \frac{\Delta t}{2\varepsilon}(J^{n+1} + J^n) \qquad (2.18)$$

By replacing equation (2.17) in (2.18) and taking E^{n+1} to the left side, it is clearly shown that E^{n+1} depends only on previous time steps and can be incorporated in FDTD scheme as:

$$E^{n+1} = \boldsymbol{A}E^n + \boldsymbol{B}\delta\left\{H^{n+\frac{1}{2}}\right\} + \boldsymbol{C}J^n \qquad (2.19)$$

where, $\boldsymbol{A} = \frac{\frac{\varepsilon}{\Delta t} - \frac{\sigma_0 \Delta t}{2(2\tau+\Delta t)}}{\frac{\varepsilon}{\Delta t} + \frac{\sigma_0 \Delta t}{2(2\tau+\Delta t)}}$, $\boldsymbol{B} = \frac{-1}{\frac{\varepsilon}{\Delta t} + \frac{\sigma_0 \Delta t}{2(2\tau+\Delta t)}}$ and $\boldsymbol{C} = \frac{\frac{(-2\tau)}{(2\tau+\Delta t)}}{\frac{\varepsilon}{\Delta t} + \frac{\sigma_0}{2(2\tau+\Delta t)}}$.

The update equation for H fields follow as:

$$H^{n+\frac{1}{2}} = H^{n-\frac{1}{2}} - \frac{\Delta t}{\mu}\delta\{E^{n+1}\} \qquad (2.20)$$

The discretized 3-D update equations for graphene are listed below:

$$J^{n+1}_{x,(i+\frac{1}{2},j,k)} = \frac{(2\tau - \Delta t)}{(2\tau + \Delta t)} J^n_{x,(i+\frac{1}{2},j,k)} + \frac{\sigma_0 \Delta t}{(2\tau + \Delta t)}\left(E^{n+1}_{x,(i+\frac{1}{2},j,k)} + E^n_{x,(i+\frac{1}{2},j,k)}\right) \qquad (2.21)$$

$$J^{n+1}_{y,\left(i,j+\frac{1}{2},k\right)} = \frac{(2\tau - \Delta t)}{(2\tau + \Delta t)} J^n_{y,\left(i,j+\frac{1}{2},k\right)} + \frac{\sigma_0 \Delta t}{(2\tau + \Delta t)}\left(E^{n+1}_{y,\left(i,j+\frac{1}{2},k\right)} + E^n_{y,\left(i,j+\frac{1}{2},k\right)}\right) \qquad (2.22)$$

$$J^{n+1}_{z,(i,j,k+\frac{1}{2})} = \frac{(2\tau - \Delta t)}{(2\tau + \Delta t)} J^n_{z,(i,j,k+\frac{1}{2})} + \frac{\sigma_0 \Delta t}{(2\tau + \Delta t)}\left(E^{n+1}_{z,(i,j,k+\frac{1}{2})} + E^n_{z,(i,j,k+\frac{1}{2})}\right) \qquad (2.23)$$

$$E^{n+1}_{x,(i+\frac{1}{2},j,k)} = \frac{\frac{\varepsilon}{\Delta t} - \frac{\sigma_0}{2(2\tau+\Delta t)}}{\frac{\varepsilon}{\Delta t} + \frac{\sigma_0}{2(2\tau+\Delta t)}} E^{n}_{x,(i+\frac{1}{2},j,k)} + \frac{-1}{\frac{\varepsilon}{\Delta t} + \frac{\sigma_0}{2(2\tau+\Delta t)}} \left[\frac{H^{n+\frac{1}{2}}_{z,\left(i+\frac{1}{2},j+\frac{1}{2},k\right)} - H^{n+\frac{1}{2}}_{z,\left(i+\frac{1}{2},j-\frac{1}{2},k\right)}}{\Delta y} - \frac{H^{n+\frac{1}{2}}_{y,(i+\frac{1}{2},j,k+\frac{1}{2})} - H^{n+\frac{1}{2}}_{y,(i+\frac{1}{2},j,k-\frac{1}{2})}}{\Delta z} \right]$$

$$+ \frac{\frac{(-2\tau)}{(2\tau+\Delta t)}}{\frac{\varepsilon}{\Delta t} + \frac{\sigma_0}{2(2\tau+\Delta t)}} J^{n}_{x,(i+\frac{1}{2},j,k)} \qquad (2.24)$$

$$E^{n+1}_{y,(i,j+\frac{1}{2},k)} = \frac{\frac{\varepsilon}{\Delta t} - \frac{\sigma_0}{2(2\tau+\Delta t)}}{\frac{\varepsilon}{\Delta t} + \frac{\sigma_0}{2(2\tau+\Delta t)}} E^{n}_{y,(i,j+\frac{1}{2},k)} + \frac{-1}{\frac{\varepsilon}{\Delta t} + \frac{\sigma_0}{2(2\tau+\Delta t)}} \left[\frac{H^{n+\frac{1}{2}}_{x,\left(i,j+\frac{1}{2},k+\frac{1}{2}\right)} - H^{n+\frac{1}{2}}_{x,\left(i,j+\frac{1}{2},k-\frac{1}{2}\right)}}{\Delta z} - \frac{H^{n+\frac{1}{2}}_{z,(i+\frac{1}{2},j+\frac{1}{2},k)} - H^{n+\frac{1}{2}}_{z,(i-\frac{1}{2},j+\frac{1}{2},k)}}{\Delta x} \right]$$

$$+ \frac{\frac{(-2\tau)}{(2\tau+\Delta t)}}{\frac{\varepsilon}{\Delta t} + \frac{\sigma_0}{2(2\tau+\Delta t)}} J^{n}_{y,(i,j+\frac{1}{2},k)} \qquad (2.25)$$

$$E^{n+1}_{z,(i,j,k+\frac{1}{2})} = \frac{\frac{\varepsilon}{\Delta t} - \frac{\sigma_0}{2(2\tau+\Delta t)}}{\frac{\varepsilon}{\Delta t} + \frac{\sigma_0}{2(2\tau+\Delta t)}} E^{n}_{z,(i,j,k+\frac{1}{2})} + \frac{-1}{\frac{\varepsilon}{\Delta t} + \frac{\sigma_0}{2(2\tau+\Delta t)}} \left[\frac{H^{n+\frac{1}{2}}_{y,\left(i+\frac{1}{2},j,k+\frac{1}{2}\right)} - H^{n+\frac{1}{2}}_{y,\left(i-\frac{1}{2},j,k-\frac{1}{2}\right)}}{\Delta x} - \frac{H^{n+\frac{1}{2}}_{x,(i,j+\frac{1}{2},k+\frac{1}{2})} - H^{n+\frac{1}{2}}_{x,(i,j-\frac{1}{2},k+\frac{1}{2})}}{\Delta y} \right]$$

$$+ \frac{\frac{(-2\tau)}{(2\tau+\Delta t)}}{\frac{\varepsilon}{\Delta t} + \frac{\sigma_0}{2(2\tau+\Delta t)}} J^{n}_{z,(i,j,k+\frac{1}{2})} \qquad (2.26)$$

The update equations for H field remain the same as in (2.12a) - (2.12c).

2.5 Stability Analysis: Intra-band Conductivity

Stability analysis is calculated via well-known Von Neumann method, which involves substituting a discrete traveling wave solution $u = e^{j(\omega n\Delta t - k_{\emptyset}\Delta\emptyset)}$, where $j = \sqrt{-1}$ and $\emptyset$ is direction: x, y or z into FDTD equations (2.21)-(2.26) and rewriting them into matrix format $Ax = 0$. In order to derive the characteristic polynomial consequently, we set $\det(A = 0)$, for dispersion relationship we will have (see Appendix A):

$$\left(\alpha e^{-j0.5\omega\Delta t} - e^{j0.5\omega\Delta t}\right)\left(4sin^2\left(\frac{\omega\Delta t}{2}\right)\right) - 4\frac{\Delta t^2 c^2}{\Delta x^2}sin^2\left(\frac{k_x\Delta x}{2}\right) - 4\frac{\Delta t^2 c^2}{\Delta y^2}sin^2\left(\frac{k_y\Delta y}{2}\right) - 4\frac{\Delta t^2 c^2}{\Delta z^2}sin^2\left(\frac{k_z\Delta z}{2}\right) + 4j\beta\frac{\Delta t}{\varepsilon}cos^2\left(\frac{\omega\Delta t}{2}\right)sin\left(\frac{\Delta t}{2}\right) = 0, \quad (2.27)$$

where $c_0 = 1/\sqrt{\varepsilon_0\mu_0}$ is the speed of light. Equation (2.27) can be further simplified by substituting the growth factor $g = e^{j\omega\Delta t}$ in to the equation, and rewriting sin and cos in terms of g:

$$ag^3 + bg^2 + cg + d = 0, \quad (2.28)$$

where,

$$a = \beta\frac{\Delta t}{2\varepsilon} + 1 \quad (2.29)$$

$$b = \beta\frac{\Delta t}{2\varepsilon} - \alpha + D - 2 \quad (2.30)$$

$$c = 1 - (D-2)\alpha - \beta\frac{\Delta t}{2\varepsilon} \quad (2.31)$$

$$d = -\alpha - \beta\frac{\Delta t}{2\varepsilon} \quad (2.32)$$

and

$$D = 4\left(\frac{\Delta t^2 c^2}{\Delta x^2}sin^2\left(\frac{k_x\Delta x}{2}\right) + \frac{\Delta t^2 c^2}{\Delta y^2}sin^2\left(\frac{k_y\Delta y}{2}\right) + \frac{\Delta t^2 c^2}{\Delta z^2}sin^2\left(\frac{k_z\Delta z}{2}\right)\right). \quad (2.33)$$

The stability condition is met if the growth factor g is less than or equal to 1. In order to derive a closed form stability criteria for equation (2.28), the Routh-Hurwitz criterion is used here. This criterion considers a mapping transformation $g = \frac{r+1}{r-1}$, which maps the exterior of the unit circle for g in the z-plane to the right half of the r-plane. For our scheme to be stable, there should be no roots in the right half plane of the r-plane.

Applying the transformation to (2.28), we will have:

$$a_3 r^3 + a_2 r^2 + a_1 r + a_0 = 0, \tag{2.34}$$

where,

$$a_3 = a + b + c + d = D(1 - \alpha), \tag{2.35a}$$

$$a_2 = 3a + b - c - 3d = 4\beta \frac{\Delta t}{\varepsilon} + D(1 + \alpha), \tag{2.35b}$$

$$a_1 = 3a - b - c + 3d = (D - 4)(\alpha - 1), \tag{2.35c}$$

$$a_0 = (4 - D)(1 - \alpha). \tag{2.35d}$$

A Routh table [31] is constructed:

Table(2) : Routh table for equation (2.34).

$\boldsymbol{a_3}$	$\boldsymbol{a_1}$
$\boldsymbol{a_2}$	a_0
$\boldsymbol{a_{1-\frac{a_3 a_0}{a_2}}}$	0
$\boldsymbol{a_0}$	0

For stability, the first column of the Routh table needs to be non-negative. Given that τ and σ_0 are both positive values, the following condition will be obtained:

$$\frac{\Delta t^2 c^2}{\Delta x^2} sin^2\left(\frac{k_x \Delta x}{2}\right) + \frac{\Delta t^2 c^2}{\Delta y^2} sin^2\left(\frac{k_y \Delta y}{2}\right) + \frac{\Delta t^2 c^2}{\Delta z^2} sin^2\left(\frac{k_z \Delta z}{2}\right) < 1. \qquad (2.36)$$

To simplify the expression, assuming the maximum value of $sin^2\left(\frac{k_x \Delta x}{2}\right) = sin^2\left(\frac{k_x \Delta x}{2}\right) = sin^2\left(\frac{k_x \Delta x}{2}\right) = 1$, the stability condition will be:

$$S = \frac{\Delta t^2 c^2}{\Delta x^2} + \frac{\Delta t^2 c^2}{\Delta x^2} + \frac{\Delta t^2 c^2}{\Delta x^2} < 1 \qquad (2.37)$$

which is the Courant–Friedrichs–Lewy (CFL) limit of the regular 3-D FTD update equations.

2.6 Conclusion

In this chapter, we introduced a conductivity model of graphene and the simplified formulations for both inter-band and intra-band conductivity. An introduction of the FDTD method followed by a basic FDTD modelling for graphene considering only inter-band conductivity model was also introduced. Then we performed Von Neuman stability analysis to show that the stability condition for the graphene update equations is the same as the CFL limit for the conventional FDTD method. The stability condition for the 1-D and 2-D case can be derived following the same method. A more detailed derivation of the stability condition is provided in Appendix A.

Chapter 3

Finite-Element-Time-Domain Method for Dispersive Medium

3.1 Introduction

To overcome the stair casing error and other limitations inherent to the FDTD method introduced in chapter 2, the hybrid method with finite element method (FEM) is proposed in this chapter. The finite-element time-domain (FETD or TDFEM) method is a very powerful numerical time domain method for solving Maxwell's differential equations. FETD unlike the FDTD is able to treat unstructured grids, which enables versatility in modeling complex geometries [40]. In general, there are two categories for FETD scheme. The first category discretizes the second-order vector wave (curl-curl) equation (VWE), obtained by eliminating one of the field variables from Maxwell's equations. It is an implicit method in which time step is not constrained by a stability criterion. This VWE-FETD has more computational complexity meaning that the solution of a linear system of equations is required at each time step. Furthermore, it can be formulated to be unconditionally stable and can be extended to higher-orders [41-42].

The second category directly discretizes the time-dependent coupled Maxwell's equations called mixed method, yielding an explicit, conditionally stable algorithm in which the maximum

time-step must be constrained to ensure stability. This method can be considered as a generalization of the finite-difference time-domain (FDTD) method for unstructured grids [43-44].

In this chapter, we first introduce a FETD formulation and a hybrid FDTD-FETD method for developing an efficient technique with better stability to solve electromagnetic problems for graphene.

Moreover, some efforts have been made to improve the stability criteria arising in the FDTD solution, which is often more severe and limiting in dispersive cases. In the following sections, some important aspects of the FETD and FDTD formulations are discussed and reviewed.

3.2 VWE-FETD Formulation

Considering the first category, the vector wave equation (VWE) in dispersive media, based on electric field and current density J_i is:

$$\nabla \times \left(\frac{1}{\mu}\nabla \times E(t)\right) + \varepsilon(t) * \frac{\partial^2 E(t)}{\partial t^2} + \frac{\partial J_i(t)}{\partial t} = 0, \qquad (3.1)$$

where $*$ denotes convolution in time. μ and ε represents the permeability and permittivity of the medium in the time domain. For a unique solution, by considering the Dirichlet boundary condition of surface S enclosed computational domain Ω [42], we will have the weak formulation of equation (3.1) as:

$$\iiint_v \left[\frac{1}{\mu} * (\nabla \times N).\left(\nabla \times E(t)\right) + N.\varepsilon(\mathrm{t}) * \frac{\partial^2 E(t)}{\partial t^2}\right] dv - \iiint_v N.\frac{\partial\left(J_i(t)\right)}{\partial t} dv = 0 \quad (3.2)$$

where, N is a vector basis function. Then, the electric field is expanded in space using vector basis function,

$$E(t) = \sum_{i=1}^{N_{edge}} N_i E_i(t) \qquad (3.3)$$

With N_{edge} indicating total number of edges (unknowns). $E_i(t)$ and N_i are the time-dependent electric field intensity and the vector basis function corresponding to the i-th degree-of-freedom (DoF), respectively.

Consequently, we will have a system of ordinary differential equations (ODE's):

$$[T]\frac{d^2\{e\}}{dt^2} + [S]\{e\} = \{f\} \qquad (3.4)$$

where, $\{e\} = \left[e_1(t), e_2(t), \ldots e_{N_{edge}}(t)\right]^T$,

$$T_{k,ij} = \iiint_v N_i . N_j \, dv, \qquad (3.5)$$

$$S_{k,ij} = \iiint_v \nabla \times N_i . \nabla \times N_j \, dv, \qquad (3.6)$$

$$f_i(t) = -\iiint_v N_i \frac{\partial J_i(t)}{\partial t} \, dv. \qquad (3.7)$$

3.3 Mixed-FETD Formulation

In the mixed FETD which directly discretize coupled Maxwell's equation, the electric field components are expanded using Whitney 1-form for edge elements and magnetic field components are expanded using Whitney 2-form basis functions for face elements [45]. This discretization leads to semi-discrete first order systems of Ordinary Differential Equation (ODE) in time:

$$\begin{cases} [T]\dfrac{d\{e\}}{dt} = [C]^T\left[T_f\right]\{b\} \\ \dfrac{d\{b\}}{dt} = -[C]\{e\} \end{cases} \qquad (3.8)$$

where $\{e\} = [e_1, e_2, \dots e_N]^T$ is electric field intensity unknowns and $\{b\} = \left[b_1, b_2, \dots b_{N_f}\right]^T$ denotes the magnetic flux density unknowns. $[C]$ represents incident matrix, which is sparse and has -1, 0 or +1 entries, and $[T]$, $\left[T_f\right]$, $[S]$ are square matrices given by:

$$T_{ij} = \int \epsilon W_i^{(1)}.W_j^{(1)}\, d\Omega \qquad (3.9)$$

$$S_{ij} = \int \nabla \times W_i^1.\nabla \times W_j^{(1)}\, d\Omega \qquad (3.10)$$

$$T_{f,ij} = \int \mu^{-1} W_i^{(2)}.W_j^{(2)}\, d\Omega \qquad (3.11)$$

in which $W^{(1)}$ and $W^{(2)}$ represent the Whitney 1-form and Whitney 2-form elements, respectively.

3.4 The Equivalence between Mixed-FETD and VWE- FETD

By eliminating {b} in equation (3.8), we obtain VWE-FETD formulation:

$$[T]\frac{d^2\{e\}}{dt^2} + [S]\{e\} = \{f\} \qquad (3.12)$$

in which it can be shown that $[S] = [C]^T\left[T_f\right][C]$ for Whitney elements [44]. Therefore, both formulations become equivalent to each other in the continuous-time case [45].

If the $[T]$ and $[T_f]$ matrices, and $[S]$ in 3-D case, are approximated using the trapezoidal integration rule, it can be shown that equation (3.1) can exactly lead to the standard FDTD equations in space [46]. See Appendix B for more details.

3.4.1 Discretization of the Dispersive Medium using Möbius Transformation

As briefly explained above, in time-harmonic form, one can account for transforming the frequency dependence of permittivity $D(\omega) = \varepsilon(\omega)E(\omega)$ into time-domain. The multiplication of harmonic functions is equivalent to convolution in the time domain. Therefore, it requires some additional effort to model these types of dispersive materials. Since the susceptibility function of a general dispersive medium can be expressed as a sum of some rational functions in the frequency domain, its time-domain counterpart inherits the feature of exponential functions.

In the Laplace space, we consider a linear permittivity model of the following form:

$$\varepsilon(s) = \frac{a_n s^n + a_{n-1} s^{n-1} + \cdots + a_1 s + a_0}{b_n s^n + b_{n-1} s^{n-1} + \cdots + b_1 s + b_0} \qquad (3.12)$$

In time domain, we will have:

$$\varepsilon(t) = \frac{a_n \mathfrak{D}^n + a_{n-1} \mathfrak{D}^{n-1} + \cdots + a_1 \mathfrak{D} + a_0}{b_n \mathfrak{D}^n + b_{n-1} \mathfrak{D}^{n-1} + \cdots + b_1 \mathfrak{D} + b_0} \qquad (3.13)$$

where $\mathfrak{D}^n$ represents, n-th derivative with respect to time ($\frac{\partial^n}{\partial t^n}$). In order to discretize equation (3.13) in time, we use the Möbius transformation technique defined as:

$$\frac{\partial}{\partial t} \rightarrow \frac{2}{\Delta t} \frac{1 - z^{-1}}{1 + z^{-1}} \qquad (3.14)$$

which is the Trapezoidal rule with time step Δt; it gives:

$$\varepsilon(z) = \frac{c_0 + c_1 z^{-1} + \cdots + c_p z^{-p}}{1 + d_1 z^{-1} + \cdots + d_p z^{-p}} \qquad (3.15)$$

where the coefficients in equation (3.15) are related to the coefficients of equation (3.13) and Δt. Applying the z-transform and making use of its property: $z^{-m}F(z) \leftrightarrow F^{n-m}$, the time discrete form of the above equations can be obtained easily.

3.5 Stability Criteria using FETD

Applying central difference discretization scheme to equation (3.12) in general form and performing the z-transform in source-free homogenous dispersive medium, we will have [48]:

$$(z-1)^2\varepsilon(z)T\tilde{u}(z) + \Delta t^2 z s\tilde{u}(z) = 0, \qquad (3.16)$$

Since matrix $[T]$ is symmetric and positive definite, we can multiply both sides of equation (3.16) with $[T]^{-1}$ resulting in an eigenvalue problem:

$$-(z-1)^2 z^{-1}\varepsilon(z)\tilde{u}(z) = \Delta t^2 T^{-1} s\tilde{u}(z). \qquad (3.17)$$

considering $\lambda = -(z-1)^2/z$, as eigenvalue of the matrix $(\Delta t^2)[T]^{-1}[s]$.

In order to have a stable formulation in FETD, the following condition has to be satisfied [49]:

Assuming λ_{max} as the maximum value of λ, all eigenvalues of the amplification matrix have to reside inside or on the unit circle (in the z-plane).

$$\Delta t \leq \frac{\sqrt{\lambda_{max}}}{\sqrt{\rho([T]^{-1}[s])}} \qquad (3.18)$$

where $\rho(.)$ denotes the spectral radius of matrix $(.)$, which is the maximum eigenvalue of matrix (.).

3.6 Conclusion

In this chapter, VWE-FETD and Mixed-FETD have been introduced and by using the bilinear transform method, the FETD formulation based on the second-order VWE has been directly extended to include arbitrary linear dispersive media. In mixed FETD, the constitutive relations

can be updated separately from the Maxwell's curl equations; therefore, it is more convenient to include medium dispersion effect. Therefore linear dispersive media using the ADE method can be implemented and the stability criteria was examined.

Chapter 4

An Efficient and Stable FDTD Formulation for Modelling Graphene

4.1 Introduction

In this chapter, a new finite-difference time-domain (FDTD) formulation for modelling graphene is proposed, in which graphene is modelled as a resistive sheet with a frequency-dependent conductivity. The formulation is first developed in the context of the vector wave finite-element time-domain (FETD) and then reduced to the FDTD based on the equivalence between these two techniques. The obtained formulation is easy-to-implement and does not alter the original FDTD update equations. It can be applied to an existing FDTD code by simply adding a correction term to appropriate variables. One of the main contributions of our work in this chapter is analyzing the stability of the proposed formulation, which has not been done previously.

4.2 Graphene as Surface Boundary Condition in Mixed FETD-FDTD

As mentioned above, graphene is modelled as surface boundary condition. Fig. 4.1 shows a 2-D rectangular grid in which the electric field unknowns {e} are assumed to be represented by edges. Graphene can be considered as a resistive sheet on which we have:

$$\sigma_{intra} E = \hat{n} \times (H^{+} - H^{-}). \qquad (4.1)$$

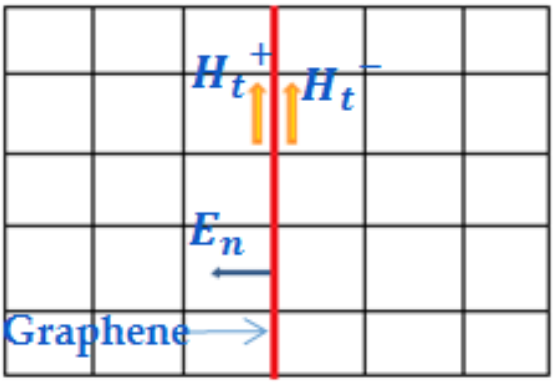

Fig.4.1 Graphene sheet in a 2-D rectangular grid.

The resistive sheet can be modeled in the VWE-FETD simply, as:

$$[T]\frac{d^2\{e\}}{dt^2} + [S]\{e\} + \{g\} = \{0\} \qquad (4.2)$$

in which

$$\{g\} = \frac{j\omega\sigma}{1 + j\omega\tau}[Q_g]\{e\} \qquad (4.3)$$

and

$$Q_{g_{ij}} = \int_{Graphene} \hat{n} \times W_i^{(1)} . \hat{n} \times W_j^{(1)} ds \qquad (4.4)$$

Equation (4.2) can be transformed into the mixed FETD formulation in which both electric $\{e\}$ and magnetic fields {b} are being updated together similar to the FDTD, as:

$$\begin{cases} [T]\dfrac{\{e\}^{n+1} - \{e\}^n}{\Delta t} = [C]^T[T_f]\{b\}^{n+\frac{1}{2}} - \{J\}^{n+\frac{1}{2}} \\ \dfrac{\{b\}^{n+\frac{3}{2}} - \{b\}^{n+\frac{1}{2}}}{\Delta t} = -[C]\{e\}^{n+1} \end{cases} \qquad (4.5)$$

where $\partial\{J\}/\partial t = \{g\}$. Applying the central difference scheme to this term yields

$$\{J\}^{n+\frac{1}{2}} = \{J\}^{n-\frac{1}{2}} + \Delta t\{g\}^n \tag{4.6}$$

In order to obtain g^n, we discretize equation (4.3) with the trapezoidal rule by simply replacing $j\omega$ with the bilinear transformation, $\frac{2}{\Delta t}\frac{1-z^{-1}}{1+z^{-1}}$ and invoking the z-transform properties, which gives:

$$\{g\}^n = \left(\frac{2\tau - \Delta t}{2\tau + \Delta t}\right)\{g\}^{n-1} + \frac{2\sigma\left[Q_g\right](\{e\}^n - \{e\}^{n-1})}{(2\tau + \Delta t)} \tag{4.7}$$

Here, we have employed the central difference to discretize the mixed FETD equation (4.5) to exactly recover the leapfrog FDTD out of it, although applying other schemes such as Crank-Nicolson (CN) or Alternating Direction Implicit (ADI) is readily possible. The trapezoidal integration has to be employed to evaluate integrals, which makes $[T]$, $[T_f]$, and $[Q_g]$ fully diagonal (mass lumping procedure). A detailed derivation of these matrices are provided in Appendix B. It should be noted that only those unknowns on which the graphene sheet lie have non-zero contribution in $[Q_g]$. Having plugged mass-lumped matrices in equation (4.5), update equations identical to the fully-discretized FDTD are obtained in which the electric field update equation for those unknowns resided on the graphene sheet have an additional term $\{J\}$. In case of an explicit FDTD method, e.g., the standard leapfrog FDTD discussed here, $\{J\}$ can be updated separately and applied as a correction term after the standard update process is performed, which greatly simplifies implementation. Needless to mention the update equation for the magnetic field is not changed in this approach.

4.3 Stability Analysis

Since our method is based on the equivalence between FETD and FDTD method, they have the same stability criteria. Therefore, for the sake of simplicity, we study the stability analysis of VWE-FETD. In order to simplify the stability analysis, we have considered a rectangular grid with the graphene on every edge of the grid. A perfect electric conductor (PEC) boundary condition is used to truncate the computational domain. Since in our grid $\Delta x = \Delta y$, both $[T]$ and $[Q_g]$ will be diagonal matrices each with the same entry on the diagonal. By substituting $[T\,] = \beta\, I$ and $[Q_g] = \varphi I$, we will have:

$$\beta I \frac{d^2\{e\}}{dt^2} + [S]\{e\} + \varphi I \frac{\sigma \mathfrak{D}}{1+\tau \mathfrak{D}}\{e\} = 0. \qquad (4.8)$$

For a square grid, $\beta = \varepsilon \Delta x^2$ and $\varphi = \Delta x$. Since $[s]$ is a symmetric matrix, it can be written as $[S] = [P]^{-1}[V][P]$. By multiplying equation (4.8) in $[P]^{-1}$ and replacing $\tilde{e} = [P]^{-1}e$ our equations will be decoupled and with λ_i as the eigenvalues of $[S]$, we will have:

$$\beta \frac{d^2\{\tilde{e}\}}{dt^2} + \lambda_i\{\tilde{e}\} + \varphi \frac{\sigma \mathfrak{D}}{1+\tau \mathfrak{D}}\{\tilde{e}\} = 0 \qquad (4.9)$$

By discretizing $\tilde{e}$ in central difference and the conductivity term via trapezoidal method we will have a third-order polynomial. By investigating the roots of the characteristic polynomial using the Routh–Hurwitz stability criterion mentioned before, and by having all eigenvalues of the amplification matrix reside inside or on the unit circle, we reach the following condition:

$$\Delta t \leq \frac{2}{\sqrt{\varphi \sigma \beta^{-1} \tau^{-1} + \beta \lambda^{-1}}} \qquad (4.10)$$

According to the definition of λ and β, $\beta^{-1}\lambda$ represents eigenvalues of $[\mathrm{T}]^{-1}[\mathrm{S}]$. The most limiting $\Delta \mathrm{t}$ is corresponding to the maximum value of $\beta^{-1}\lambda$, which is shown to be equal to

$$\beta^{-1}\lambda = \frac{4c^2}{\Delta x^2} + \frac{4c^2}{\Delta y^2} \tag{4.11}$$

for the 2-D case [50] in which c is the speed of light. As can be seen from equation (4.10), this condition reduces to the CFL condition in the absence of graphene (σ=0); however, it becomes more limiting, if graphene layers are included in simulation. In order to see how much more stringent the new condition is, we consider the ratio of the two terms in the denominator of equation (4.10).

By substituting right hand side of (4.11), $\beta = \epsilon\Delta x^2$ and $\varphi = \Delta x$, we have:

$$\frac{\varphi\sigma\beta^{-1}\tau^{-1}}{\lambda\beta^{-1}} = \frac{\mu\sigma\Delta x}{8\tau} \tag{4.12}$$

which is very small for typical graphene problems. In order to demonstrate the validity of the stability condition, we conducted a numerical experiment in which we considered a rectangular grid with 30×30 cells, Δx=Δy=2μm and PEC boundary condition on the outer boundaries. We assumed that graphene resides on every edge of the grid with T=300K, $\mu_c = 0.5\,ev$ and $\tau = 0.5\,ps$. Under this assumptions, the CFL condition yields Δt= 4.717×10^{-15} and the condition obtained from equation (4.10) gives Δt = 4.632×10^{-15}, which is less than 2 percent smaller than the CFL condition. We performed the simulation for two different values of Δt slightly below and above the value obtained from the new condition, which are Δt= 4.63×10^{-15} and Δt= 4.64×10^{-15} respectively. As can be seen in Fig. 4.2, the first Δt results in completely stable results while the second value of Δt leads to unstable results.

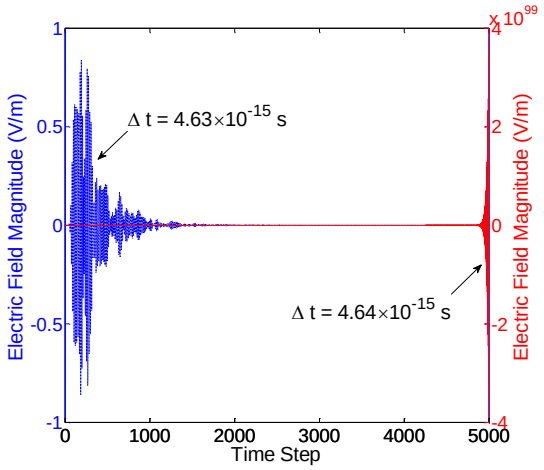

Fig. 4.2. Stability analysis; on the left: stable results with time steps slightly below the new stability condition, on the right: unstable results with time steps slightly above the new stability condition.

4.4 Numerical Results

4.4.1 Reflection and Transmission Response

In order to validate the proposed formulation, we considered two numerical examples. Our first example involves calculating reflection and transmission coefficients of an infinitely long graphene sheet with T=300K, $\mu_c = 0.5\ ev$ and $\tau = 0.5\ ps$ as in [37], located in the middle of our computational domain. The problem was solved in 2-D with 210×210 cells, $\Delta x = \Delta y = 2\mu m$. A perfect electric conductor (PEC) was used to truncate the graphene layer and a 8 cell layer perfectly matched layer (PML) for both sides of the domain. We excited the problem with a Blackman-Harris pulse shape plane-wave [28]. The exact solutions were calculated by $T = 2/(2 + \eta_0 \sigma_{gr})$ and $\Gamma = T - 1$, in which η_0 is free space impedance and σ_{gr} is graphene conductivity.

Fig. 4.3 shows comparison of the numerical and analytical results of transmission and reflection coefficients in which we can observe our method in an excellent agreement with the analytical results.

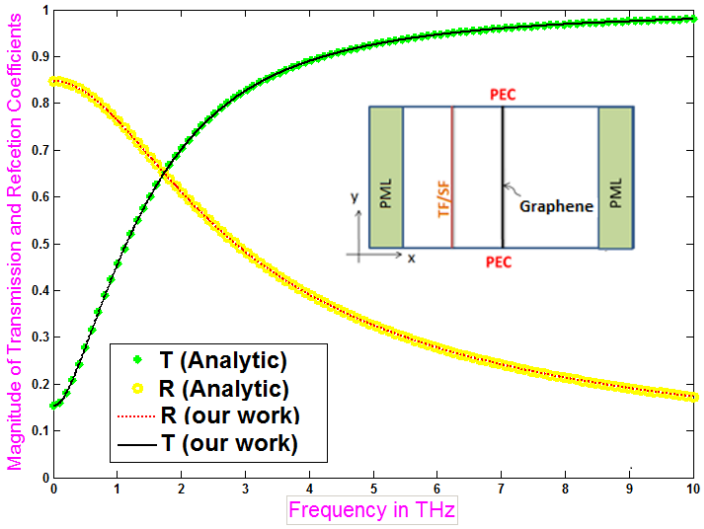

Fig. 4.3. Comparison between transmission and reflection coefficients of our numerical method and analytical results for Graphene; T=300K, τ=0.5ps, μc=0.5ev.

4.4.2 Surface Plasmon Polariton Supported by Graphene

As mentioned before, one of the main applications in which graphene plays an important role is SPP waves. The field of SPPs supported by graphene is tightly confined on the surface and the damping loss of its SPPs is relatively low, hence, the propagation length could reach dozens of wavelengths of SPPs [44]. Typically finding the electromagnetic fields in these subwavelength geometries requires numerical approaches to solve Maxwell's equations. Due to the difficulties in measuring the SPP field, numerical simulation has been the essential manner to verify the theoretical analysis. This matter leads to our second example in which, the infinite graphene sheet is excited by a sinusoidal dipole electric source as SPP surface source at 30 THz frequency. Our domain has 200×60 cells and $\Delta x = \Delta y = 20nm$. The time step is calculated as $\Delta t = \Delta x/(2c_0) = 3.3 \times 10^{-17}s$ and we truncated the domain with 8 layer PML cells. In order to avoid spurious reflections from the boundary, the graphene layer is extended to the PML regions. Fig. 4.4, shows the spatial distribution of Hz at time step 100 000 when the fields reach steady

state. From field distribution we can easily extract the guided wavelength $\lambda_{SPP} = 29 \times 20\, nm = 580\, nm$ which is in good agreement with the analytically calculated guided wavelength as $\lambda_{SPP} = \frac{\lambda_0}{\Re\left(\sqrt{1-\left(\frac{2}{\eta_0 \sigma_{gr}}\right)^2}\right)} = 586\, nm$. λ_0 is the free-space wavenumber [50].

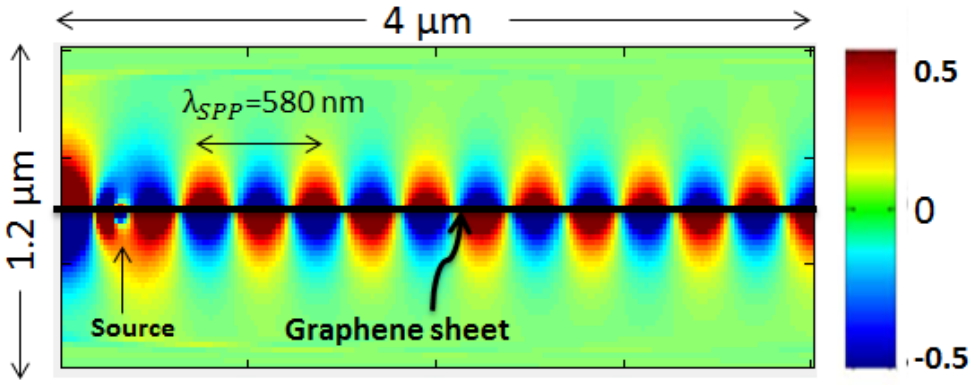

Fig. 4.4. Spatial distribution of Hz at time step 100 000 depicting SPP surface wave on the graphene layer.

4.5 Conclusion

In this chapter, we developed a simple, low cost formulation based on equivalence between FETD and FDTD to model graphene which can be implemented with minimal modifications on an existing FDTD code.

Stability analysis has been performed for the first time unlike the other methods used to model graphene. Although it is an explicit method, the CFL stability condition has only been changed negligibly.

Chapter 5

Incorporating Inter-band Conductivity into FDTD using Recursive Fast Fourier Transform

5.1 Introduction

In this chapter, an efficient method based on the recursive fast Fourier transform (FFT) to incorporate both the intra-band and inter-band conductivity terms of graphene into the finite-difference time-domain (FDTD) method is proposed. As it only requires numerical values of the conductivity, not only does it not enforce any restrictions on the conductivity models, but also can directly take into account material properties obtained from measurement. It reduces the total computational cost from $\boldsymbol{O}(\boldsymbol{N^2})$ to $\boldsymbol{O}(\boldsymbol{Nlog^2N})$ where N is the length of the unknown (e.g. edge elements). The FDTD method is also modified and proven to retain the stability condition of the standard FDTD method.

The convolution involving the logarithmic approximation of the inter-band term can't be evaluated efficiently in a recursive manner and the computation cost increases as the time-stepping proceeds [22]. Several authors have alleviated this problem by approximating the inter-band term using high-order rational functions [21,22,51]. The order of the approximating function can be very high, which consequently increases the complexity and cost of the implementation.

Furthermore, these methods require an accurate conductivity model of graphene, which may not be available in some applications such as graphene nanocomposites [37]. In these scenarios, measurement might be the primary approach to obtain electromagnetic properties in an accurate manner, which can't be directly implemented into the FDTD code.

In this chapter, we employ the recursive fast Fourier transform (FFT) to evaluate the time convolution in order to incorporate both inter-band and intra-band conductivity in the FDTD. This implementation needs only the values of the conductivity functions instead of the closed-form models as required by previous approaches. It reduces the complexity of brute-force evaluation of the convolution from $\boldsymbol{O}(\boldsymbol{N^2})$ to $\boldsymbol{O}(\boldsymbol{Nlog^2N})$. In addition, the FDTD algorithm is modified and we prove that it preserves the stability condition of the standard FDTD algorithm compared to chapter 4 where the stability condition is a little limiting. Various numerical examples are presented to validate the method.

5.2 New Formulation for Modelling Graphene in the FDTD Method

The FDTD method described here is motivated by the easy-to-implement formulation presented in chapter 4; however, the previous formulation imposes an extra constraint on the stability condition. Here, a modified formulation is presented to retain the stability condition of the standard FDTD.

By discretizing Maxwell's curl equations (2.5-2.6) in space and considering $\delta\{\cdot\}$ as the discrete curl operator, we will have the discrete form of the fields as

$$\frac{\delta\{E\}}{\mu} = -\frac{\partial H}{\partial t} \tag{5.1}$$

$$\frac{\delta\{H\}}{\varepsilon} = \frac{\partial E}{\partial t} + \frac{J}{\varepsilon}. \tag{5.2}$$

Using the leap-frog method to obtain the discrete form of equation (5.1) and equation (5.2) in time and taking the average value of J results in the following equations:

$$\frac{\delta\{E\}^{n+1}}{\mu} = -\frac{H^{n+\frac{3}{2}} - H^{n+\frac{1}{2}}}{\Delta t} \tag{5.3}$$

$$\frac{\delta\{H\}^{n+\frac{3}{2}}}{\varepsilon} = \frac{E^{n+1} - E^{n}}{\Delta t} + \frac{J^{n+1} + J^{n}}{2\varepsilon}. \tag{5.4}$$

Applying the trapezoidal integration rule to evaluate $J^n = \sigma * E^n$ over each interval, yields

$$J^n = \frac{\Delta t}{2}(\sigma^1 E^n + \sigma^n E^1) + \Delta t \sum_{m=2}^{n-1} \sigma^{n-m+1} E^m. \tag{5.5}$$

Since calculating J^n requires having the value of E^n, we take the term containing E^n out of equation (5.5) and consider the rest as

$$G^n = \frac{\Delta t}{2}(\sigma^n E^1) + \Delta t \sum_{m=2}^{n-1} \sigma^{n-m+1} E^m \tag{5.6}$$

which clearly results in

$$J^n = \frac{\Delta t}{2}(\sigma^1 E^n) + G^n. \tag{5.7}$$

Subsequently, substituting equation (5.7) into equation (5.4) and taking the E^{n+1} to the left-hand side yields;

$$E^{n+1} = \frac{1}{X}\left(\frac{\delta\{H\}^{n+\frac{3}{2}}}{\varepsilon} + \frac{E^n}{\Delta t}\right) - \frac{Y}{X} \tag{5.8}$$

in which $X = \left(1 + \frac{\Delta t^2 \sigma^1}{4\varepsilon}\right)$ and $Y = \frac{\Delta t}{2\varepsilon}(G^{n+1} + J^n)$.

As can be seen in equation (5.8), the electric field update equation for the unknowns residing on the graphene sheet will have a correction term. After the standard update process is performed,

Y can be updated separately and added to the electric field update followed by a division by the constant value of X. This approach greatly simplifies implementation without changing the standard FDTD update process. Needless to mention, the update equation for the magnetic field is not changed in this approach.

5.3 Recursive Fast Fourier Transform

Applying the trapezoidal integration rule to $J^n = \sigma(t) * E^n$ transforms the evaluation of the convolution integral into calculation of a summation with the basic form of

$$J^n = \sum_{m=1}^{n} \sigma^{n-m} E^m. \qquad (5.9)$$

In order to evaluate equation (5.9) with the recursive FFT algorithm, we need to divide equation (5.9) into summations of lengths of 2^p (except the last one) starting with N, the biggest possible 2^p, and in an descending order [28]

$$J^n = \sum_{m=1}^{N} \cdot + \sum_{m=N+1}^{N+2^{p_1}} \cdot + \sum_{m=N+2^{p_1}+1}^{N+2^{p_1}+2^{p_2}} \cdot + \cdots + \sum_{m=\cdots}^{n} \cdot$$

$$p > p_1 > p_2 > \cdots \qquad (5.10)$$

It is optimal to keep the length of 2^p-long summations equal to or greater than 64 [52]. Therefore, the length of the last summation will be less than 64, which should be evaluated directly.

In order to explain it clearly, we consider evaluation of equation (5.9) at the 890th time-step (n=890). We first break equation (5.9) into several summations each of the length $2^p; p > 5$:

$$J^{(890)} = \sum_{m=1}^{\mathbf{512}} \cdot + \sum_{m=513}^{512+\mathbf{256}} \cdot + \sum_{m=769}^{768+\mathbf{64}} \cdot + \sum_{m=833}^{832+\mathbf{58}} \cdot \qquad (5.11)$$

By breaking this summation to the lengths of 2^p , we can efficiently evaluate the first three summations using FFT. However, we need to calculate last remaining summation directly, as it is not efficient to further break a summation shorter than 64 to apply FFT which has been explained in [52].

It should be noted that only one summation has to be calculated (either directly or using FFT) at each time-step, because the length of a discrete convolution containing two vectors each with m entries is $2m-1$. For example, once we evaluate the first summation at 512th time-step, we do not need to re-evaluate it until $n = 1024$. Similarly, we do not re-evaluate the first three summations in equation (5.11) for any values of n between 833 and 895. The last two summations will be replaced by one summation from 769 to 768+128 once we reach 896, which should be evaluated by FFT. When this process is applied recursively, more convolutions can be evaluated by FFT and the total cost of evaluating the entire summation containing N steps is eventually reduced to $O(Nlog^2N)$ [12].

$$O\left(NlogN + 2\left(\frac{N}{2}log\frac{N}{2}\right) + 4(\frac{N}{4}log\frac{N}{4})\right) = O(Nlog^2N) \quad (5.12)$$

5.4 Stability Analysis

Our stability analysis is based the well-known von Neumann method, which involves substituting a traveling plane-wave trial function $E_\alpha = E_{\alpha 0}e^{-\jmath(ik_x\Delta x + jk_y\Delta y)}; \jmath = \sqrt{-1}$ into the FDTD equations and rewrite them in the form $X^{n+1} = \mathbf{\Lambda}X^n$. In order to have a non-growing solution during time stepping, the eigenvalue of $\mathbf{\Lambda}$ with the largest magnitude should not lie outside of the unit circle in the complex plane [48]. For the sake of brevity, we only study the 2-D TM_z case here for which the governing equations are

$$\frac{\partial H_x}{\partial t} = -\frac{1}{\mu}\frac{\partial E_z}{\partial y} \tag{5.13}$$

$$\frac{\partial H_y}{\partial t} = \frac{1}{\mu}\frac{\partial E_z}{\partial x} \tag{5.14}$$

$$\frac{\partial E_z}{\partial t} = \frac{1}{\varepsilon}\left(\frac{\partial H_y}{\partial x} - \frac{\partial H_x}{\partial y}\right) - J_z. \tag{5.15}$$

By discretizing equations (5.13-5.15) in space and time and substituting the trial functions, we reach

$$H_{x0}^{n+\frac{1}{2}} = H_{x0}^{n-\frac{1}{2}} - \frac{A\Delta t}{\mu} E_{z0}^{n} \tag{5.16}$$

$$H_{y0}^{n+\frac{1}{2}} = H_{y0}^{n-\frac{1}{2}} + \frac{B\Delta t}{\mu} E_{z0}^{n} \tag{5.17}$$

$$E_{z0}^{n+1} = E_{z0}^{n} + \left(\frac{B\Delta t}{\varepsilon} H_{y0}^{n+\frac{1}{2}} \quad - \frac{A\Delta t}{\varepsilon} H_{x0}^{n+\frac{1}{2}}\right) - \frac{\Delta t}{2}(J_z^{n+1} + J_z^{n}) \tag{5.18}$$

where $A = \frac{\jmath 2}{\Delta y} sin(k_y \frac{\Delta y}{2})$ and $B = \frac{\jmath 2}{\Delta x} sin(k_x \frac{\Delta x}{2})$.

In the evaluation of J_z^n, we only take into account the intra-band conductivity term $\sigma(t) = \sigma_{intra}(t) = Ke^{-\alpha t}u(t)$, as the exponential form allows us to write the time-discrete convolution in a recursive fashion. However, the non-linear inter-band term does not possess such a property and makes the stability analysis complicated. Substituting the conductivity term into equation (5.5) and making some simplifications yields the following recursive relation

$$J^{n+1} = e^{-\alpha\Delta t} J^{n} + \frac{K\Delta t}{2} e^{-\alpha\Delta t}(E^{n} + e^{\alpha\Delta t} E^{n+1}). \tag{5.19}$$

Now, we write equations (5.16-5.18) in the matrix form shown below

$$\boldsymbol{M}\left[H_x^{n+\frac{1}{2}}; H_y^{n+\frac{1}{2}}; E_z^{n+1}; J_z^{n+1}\right] = \boldsymbol{N}\left[H_x^{n-\frac{1}{2}}; H_y^{n-\frac{1}{2}}; E_z^{n}; J_z^{n}\right] \tag{5.20}$$

in which

$$\boldsymbol{M} = \begin{bmatrix} 1 & 0 & 0 & 0 \\ 0 & 1 & 0 & 0 \\ A\Delta t/\varepsilon & -B\Delta t/\varepsilon & 1 & \Delta t/2 \\ 0 & 0 & -Ke^{\alpha\Delta t}\Delta t/\varepsilon & e^{\alpha\Delta t} \end{bmatrix} \tag{5.21}$$

and

$$\boldsymbol{N} = \begin{bmatrix} 1 & 0 & -A\Delta t/\mu & 0 \\ 0 & 1 & B\Delta t/\mu & 0 \\ 0 & 0 & 1 & -\Delta t/2 \\ 0 & 0 & K\Delta t/2 & 1 \end{bmatrix}. \tag{5.22}$$

Studying the eigenvalue of $\boldsymbol{\Lambda} = \boldsymbol{M^{-1}N}$ shows that to meet $\max(|\mathrm{eig}(\boldsymbol{\Lambda})|) \leq 1$ requirement, the time step should satisfy the following condition

$$\Delta t \leq \frac{\sqrt{\mu\varepsilon}}{\sqrt{\frac{1}{\Delta x^2} + \frac{1}{\Delta y^2}}} \tag{5.23}$$

which is identical to the conventional stability condition, hence the new method does not limit the stability of the underlying FDTD method. Our stability analysis for the 3-D case yields the same result.

5.5 Numerical Results

To demonstrate the validity of the proposed formulation, we simulate the problem of plane-wave reflection by and transmission through an infinite graphene sheet with T=300K, $\mu_c = 0.6\ eV$ and $\Gamma = 11\ meV/\hbar$ [21] using the 2-D FDTD method. The graphene sheet was located inside a parallel-plate waveguide with PEC walls and was truncated by a 10-layer thick perfectly matched layer (PML). As shown in Fig. 5.1, the computational domain contains 200×200 cells with $\Delta x = \Delta y = 2\mu m$.

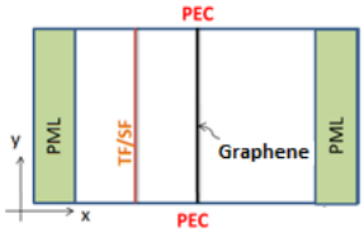

Fig. 5.1. Graphene sheet in 2-D FDTD computational domain truncated by PML and PEC boundaries.

5.5.1 Reflection and Transmission Response

The transmission and reflection coefficients are obtained using discrete Fourier transform and are compared with the analytical solutions calculated by $Tr = 2/(2 + \eta_0 \sigma_{gr})$ and $\Gamma = Tr - 1$, in which η_0 is free space impedance and σ_{gr} is the graphene conductivity including both inter-band and intra-band terms.

Fig. 5.2 shows a comparison of the numerical and analytical results, for both the transmission and reflection coefficients; it demonstrates excellent agreement with the proposed method. The relative error between the analytical results and the proposed method is less than 0.05% in the considered frequency range.

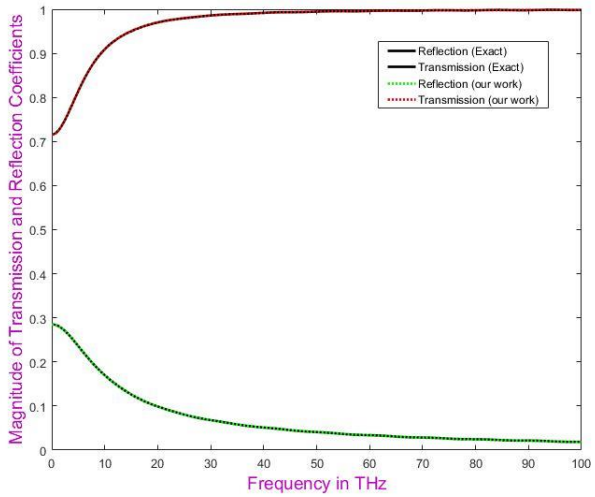

Fig. 5.2. Comparison between transmission and reflection coefficients for a normally incident plane-wave.

5.5.2 TM Surface Plasmon Polariton

Since graphene supports TM surface plasmon polariton (SPP) waves [53], it gives rise to micrometer size antennas resonating in the terahertz frequency range, yielding an advantage over their metallic counterparts. For this reason, as a second example, we simulate a SPP surface wave on two graphene layers excited by a sinusoidal dipole electric source at 30 THz frequency, as the SPP surface source in between the layers.

Fig. 5.3. Shows the spatial distribution of E_z at time step 40,000 when the field reaches steady-state. Our domain has 120×200 cells and Δx = Δy = 20 nm. The time step is calculated as Δt = $\Delta x/(2c_0) = 3.3 \times 10^{-17}$ s. In order to avoid spurious reflections from the boundary, the graphene layer is extended to PML regions of 10 cells. From the field distribution, we can easily extract the guided wavelength $\lambda_{SPP} = 29 \times 20 = 580\, nm$ while the results of the analytically calculated guided wavelength is $\lambda_{SPP} = \frac{\lambda_0}{re\sqrt{1-(\frac{2}{\eta_0 \sigma_{gr}})^2}} = 577\ nm.$

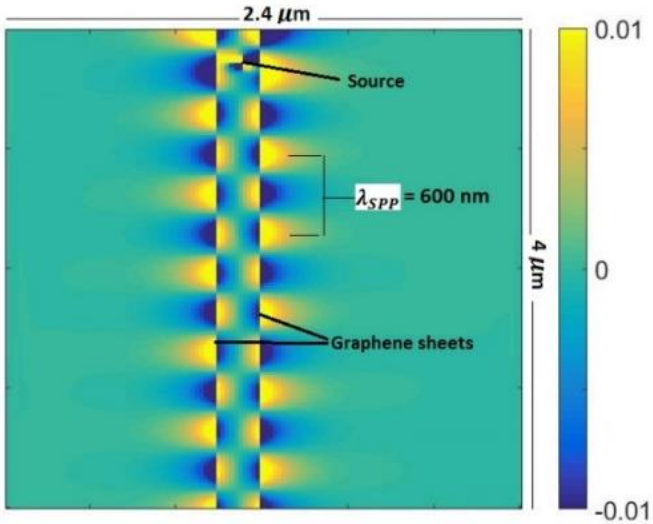

Fig. 5.3. Shows the calculated field of the SPP-mode propagating along two graphene sheets with the dipole source located in between.

5.6 Conclusion

This work presents an efficient method to model graphene layers based on the recursive fast Fourier transform (FFT), in which both the intra-band and inter-band terms of its surface conductivity are modeled. This new approach only requires numerical values of the conductivity directly obtained from measurement, as opposed to the exact conductivity model required by previous methods. It is also shown to be fast and very cost effective.

Moreover, the new FDTD method can be implemented with minimal modifications using an existing code and leaves the stability condition of the underlying FDTD method intact.

Chapter 6

Conclusion and Future Work

6.1 Conclusion

In this thesis we focused on modelling graphene in time domain techniques based on the simplified formulations for both inter-band and intra-band conductivities. First, a basic FDTD modelling for graphene considering only inter-band conductivity model was introduced. Then we performed Von Neuman stability analysis to show that the stability condition for the graphene update equations is the same as the CFL limit for the conventional FDTD method.

Furthermore, VWE-FETD and Mixed-FETD have been introduced and, by using the bilinear transform method, the FETD formulation based on the second-order VWE has been directly extended to include arbitrary linear dispersive media. In mixed FETD, the constitutive relations can be updated separately from the Maxwell's curl equations; therefore, it is more convenient to include the medium dispersion effect. Therefore linear dispersive media using the ADE method can be implemented and the stability criteria was examined. In addition, a simple, low cost formulation has been developed based on equivalence between FETD and FDTD to model graphene which can be implemented with minimal modifications on an existing FDTD code. For the first time stability analysis has been performed unlike the other methods used to model

graphene. Although it is an explicit method, the CFL stability condition has only been changed negligibly.

In order to take into account the inter-band conductivity model as well, an efficient method to model graphene layers based on the recursive fast Fourier transform (FFT), in which both the intra-band and inter-band terms of its surface conductivity are modeled. This new approach only requires numerical values of the conductivity directly obtained from measurement, as opposed to the exact conductivity model required by previous methods. It is also shown to be fast and very cost effective. Moreover, the new FDTD method can be implemented with minimal modifications using an existing code and leaves the stability condition of the underlying FDTD method intact.

6.2 Future Work

In the future works, developing unconditionally stable numerical methods such as Crank-Nicolson or a hybrid implicit explicit-finite difference time-domain (HIE-FDTD) for a stability-improved implementation where both the inter-band and intra-band conductivity of the graphene are handled directly through an auxiliary difference is an interesting possibility.

Graphene has a promising future in optical devices operating at the high terahertz frequency range graphene nanoribbons (GNR) in which the inter-band conductivity need to be taken into consideration. In those cases, higher computational efficiency such as discontinuous Galerkin time-domain (DGTD) algorithm using a nonlocal transparent surface impedance boundary condition (SIBC) incorporated into the DGTD scheme will be an interesting modelling approach.

References

[1] K. S. Novoselov, V. I.Fal'ko, L.Colombo, P.R.Gellert,M. G. Schwab, and K. Kim, "A roadmap for graphene," Nature, vol. 490, no. 7419, pp. 192–200, Oct. 2012.

[2] S. Nazarpour, S. R. Waite "Graphene Technology: From Laboratory to Fabrication" John Wiley &sons, Sep. 2016.

[3] M. Dragoman, D. Neculoiu, D. Dragoman, G. Deligeorgis, G. Konstantinidis, A. Cismaru, F. Coccetti, and R. Plana, "Graphene for microwaves," Microwave Magazine, IEEE, vol. 11, no. 7, pp. 81 –86, Dec. 2010.

[4] C. Lee, X. Wei, J. Kysar, and J. Hone, "Measurement of the elastic properties and intrinsic strength of monolayer graphene." Science, vol. 321, p. 385388, 2008.

[5] Bunch, J. Scott, et al. "Impermeable atomic membranes from graphene sheets." Nano letters, vol. 8, no. 8, pp. 2458-2462, 2008.

[6] A. Geim, "Graphene: Status and prospects," Science, vol. 324, no. 5934, pp. 1530–1534, June. 2009.

[7] D. Dikin and et al, "Preparation and characterization of graphene oxide paper," Nature, vol. 448, pp. 457–460, 2007.

[8] Zhao, Weifeng, et al. "Preparation of graphene by exfoliation of graphite using wet ball milling." Journal of Materials Chemistry, vol. 20, no .28, pp. 5817-5819, 2010.

[9] Reina, Alfonso, et al. "Large area, few-layer graphene films on arbitrary substrates by chemical vapor deposition." Nano letters, vol. 9, no. 1,pp. 30-35, 2008.

[10] Arrieta, Javier Munárriz. Modelling of Plasmonic and Graphene Nanodevices. Springer, 2014.

[11] Kumar, Akshay, and Chongwu Zhou. "The race to replace tin-doped indium oxide: which material will win?." ACS nano 4.1, pp. 11-14, 2010.

[12] K. Kim and et al, “Large-scale pattern growth of graphene films for stretchable transparent electrodes,” Nature, vol. 457, pp. 706–710, Feb. 2009.

[13] S. Bae and et al, “Roll-to-roll production of 30 inch graphene films for transparent electrodes,” Nat. Natechnol., vol. 5, p. 574578, Jun. 2010.

[14] Schwierz, Frank. "Graphene transistors." Nature nanotechnology, vol. 5, no .7, pp. 487-496, 2010.

[15] P. Russer, N. Fichtner, P. Lugli, W. Porod, J. Russer, and H. Yordanov, “Nanoelectronicsbased integrate antennas,” Microwave Magazine, IEEE, vol. 11, no. 7, pp. 58 –71, Dec. 2010

[16] Lu, Hua, et al. "Graphene-based active slow surface plasmon polaritons." Scientific reports vol. 5, pp. 8443, 2015.

[17] Vakil, Ashkan, and Nader Engheta. "Transformation optics using graphene." Science, vol. 332, no .6035, pp. 1291-1294, 2011.

[18] G. W. Hanson, “Dyadic Green’s functions and guided surface waves for a surface conductivity model of graphene,” J. Appl. Phys., Vol. 103, 064302, 2008.

[19] A. Fallahi and J. Perruisseau-Carrier, “Design of tunable biperiodic graphene meta-surfaces,” Phys. Rev. B, vol. 86, no. 19, pp. 195408–195408, Nov. 2012.

[20] R. Filter, *et al*, “Tunable graphene antennas for selective enhancement of THz emission,” Opt. Express, vol. 21, no. 3, pp. 3737–3745, Feb. 2013.

[21] A. Mock, “Pade approximant spectral fit for FDTD simulation of Graphene in the near infrared,” Opt. Mater. Exp., Vol 2, 164810, 2012.

[22] H. Lim et al, “FDTD modeling of graphene devices using complex conjugate dispersion material model,” IEEE Microwave Wireless Comp. Lett., Vol. 22, 612-614, 2012.

[23] G. D. Bouzianas, N. V. Kantartzis, C. S. Antonopoulos, and T. D. Tsiboukis “Optimal modeling of infinite graphene sheets via a class of generalized FDTD schemes,” IEEE Trans. Magn., Vol. 48, 379–382, 2012.

[24] V. Nayyeri, M. Soleimani, and O. M. Ramahi, “Modeling Graphene in the Finite-Difference Time-Domain Method Using a Surface Boundary Condition,” IEEE Trans. Antennas Propagat., vol. 61, no. 8, pp. 4176–4182, Aug. 2013.

[25] D. J. Riley and N. W. Riley, “First order models for thin-material sheets and coatings in the finite element time-domain method,” IEEE AP-S Int. Symp. Dig., vol. 4, pp. 3489–3492, June 2004.

[26] CST Studio Suite, [Online]. Available: http://www.cst.com

[27] COMSOL Multiphysics, [Online]. Available: http://www.comsol.com

[28] A. Taflove and S. C. Hagness, “Computational Electrodynamics: The Finite-Difference Time-Domain Method”. Norwood, MA, USA: Artech House, 2000.

[29] J. B. Schneider. "Understanding the finite-difference time-domain method." School of electrical engineering and computer science Washington State University, 2010.

[30] Yee, Kane. "Numerical solution of initial boundary value problems involving Maxwell's equations in isotropic media." IEEE Transactions on antennas and propagation, vol. 14, no.3, pp. 302-307, 1966.

[31] A. Pereda, L. Vielva, A. Vegas, and A. Prieto, “Analyzing the stability of the FDTD technique by combining the von neumann method with the routh-hurwitz criterion,” Microwave Theory and Techniques, IEEE Transactions on, vol. 49, no. 2, pp. 377 –381, Feb

2001.

[32] X. Yu and C. D. Sarris, “A perfectly matched layer for subcell FDTD and applications to the modeling of graphene structures,” IEEE Antennas Wireless Propag. Lett., vol. 11, pp. 1080–1083, 2012.

[33] J. G. Maloney and G. S. Smith, “The use of surface impedance concepts in the finite-difference time-domain method,” IEEE Trans. Antennas Propag., vol. 40, no. 1, pp. 38–48, Jan. 1992.

[34] J. H. Beggs, R. J. Luebbers, K. S. Yee, and K. S. Kunz, “Finite-difference time-domain implementation of surface impedance boundary conditions,” IEEE Trans. Antennas Propag., vol. 40, no. 1, pp. 49–56, Jan. 1992.

[35] L. Wu and L. Han, “Implementation and application of resistive sheet boundary condition in the finite-difference time-domain method,” IEEE Trans. Antennas Propag., vol. 40, no. 6, pp. 628–633, Jun. 1992.

[36] J. G. Maloney and G. S. Smith, “A comparison of methods for modeling electrically thin dielectric and conducting sheets in the finite-difference time-domain method,” IEEE Trans. Antennas Propag., vol. 41, no. 5, pp. 690–694, May 1993.

[37] V. P. Gusynin, S. G. Sharapov, and J. P. Carbotte, “Magneto-optical conductivity in graphene,” J. Phys., Condens. Matter, vol. 19, no. 2, pp. 026222, Jan. 2007.

[38] G. W. Hanson, “Dyadic greens functions and guided surface waves for a surface conductivity model of graphene,” Journal of Applied Physics, vol. 103, no. 064302, Mar. 2008.

[39] A. Taflove and S. C. Hagness, Computational Electrodynamics, “The Finite-Difference Time-Domain Method”, 3rd ed. Boston, MA, USA, Artech House, 2005.

[40] J.F. Lee, R. Lee, and A. Cangellaris, “Time-domian finite-element methods,” IEEE Trns. Antennas Propag, vol 45. Pp. 430-442, March 1997.

[41] O. Zienkiewicz and R. Taylor, The Finite Element Method, 4th ed., New York: McGraw-Hill, 1988.

[42] J. M. Jin, The Finite Element Method in Electromagnetics, 2nd ed., New York: Wiley, 2002.

[43] C. Chan, J. Elson, and H. Sangani, "An explicit finite-difference time-domain method using Whitney elements," Proc. IEEE APS Int. Symp. Dig., vol. 3, pp. 1768-1771, Jul. 1994.

[44] M. F. Wong, O. Picon, and V. Hanna, "A finite element method based on Whitney forms to solve Maxwell equations in the time domain," IEEE Trans. on Magnetics, vol. 31, no. 3, pp. 1618-1621, May 1995.

[45] A. Akbarzadeh-Sharbaf D. D. Giannacopoulos "Finite-element time-domain solution of the vector wave equation in doubly dispersive media using Möbius transformation technique" IEEE Trans. Antennas Propag. Vol. 61, No. 8, 4158-4166, 2013.

[46] J.-F. Lee and Z. Sacks, ”Whitney elements time domain (WETD) methods," IEEE Trans. Magn., vol. 31, pp. 1325-1329, May 1995.

[47] G. Cohen and P. Monk, “Gauss point mass lumping schemes for Maxwell’s equations,” Numer. Methods Partial Differ. Equ., vol. 14, no. 1, pp. 63–88, 1998.

[48] D. Jiao and J.-M. Jin, “A general approach for the stability analysis of the time-domain finite-element method for electromagnetic simulations,” IEEE Trans. Antennas Propag., vol. 50, no. 11, pp. 1624–1632, Nov. 2002.

[49] S. Wang and F. L. Teixeira, \Some remarks on the stability of time-domain electromagnetic simulations," IEEE Trans. Antennas Propag., vol. 52, pp. 895-898, Mar.2004.

[50] F. Edelvik, R. Schuhmann, and T. Weiland, “A general stability analysis of FIT/FDTD applied to lossy dielectrics and lumped elements,” Int. J. Numer. Model., Electron. Netw., Devices, Fields, vol. 17, no. 4, pp. 407–419, 2004.

[51] Nayyeri, V., M. Soleimani, and O. M. Ramahi, “Wideband modeling of graphene using the finitedifference time-domain method,” IEEE Trans. Antennas Propag., Vol. 61, No. 12, 6107–6114, Dec. 2013.

[52] Chiang, I-T. and W. C. Chew, “Fast real-time convolution algorithm for microwave multiport networks with nonlinear terminations,” IEEE Trans. Circuits Syst-II: Express Briefs, Vol. 52, No. 7, 370–375, Jul. 2005.

[53] Wang, B., X. Zhang, X. Yuan, and J. Teng, “Optical coupling of surface plasmons between graphene sheets,” Appl. Phys. Lett., Vol. 100, No. 13, 131111, 2012.

Appendix A

Dispersion Relation Derivation

Substituting the travel wave expression of $U = \widetilde{U}e^{j(\omega\Delta t - k_\emptyset \Delta\emptyset)}$ in, $k_\emptyset \Delta\emptyset = k_x i\Delta x + k_y j\Delta y + k_z k\Delta z$ to equation (2.21-2.26) and equations (2.12a-2.12c) and simplifying the equations, we will have:

$$e^{j(\omega(n+1)\Delta t)}\, e^{j(k_\emptyset \Delta\emptyset)}\, \tilde{J}_x = \alpha e^{j(\omega\Delta t)}\, e^{j(k_\emptyset \Delta\emptyset)}\, \check{J}_x + e^{j(k_\emptyset \Delta\emptyset)}\, \beta\left(e^{j(\omega(n+1)\Delta t)}\, \tilde{E}_x + e^{j(\omega n\Delta t)}\, \tilde{E}_x \right)$$

$$\rightarrow (e^{j(\omega\Delta t)} - \alpha)\tilde{J}_x - \beta(e^{j(\omega\Delta t)} + 1)\tilde{E}_x = 0 \qquad (A.1)$$

$$(e^{j(\omega\Delta t)} - \alpha)\tilde{J}_y - \beta(e^{j(\omega\Delta t)} + 1)\tilde{E}_y = 0 \qquad (A.2)$$

$$(e^{j(\omega\Delta t)} - \alpha)\tilde{J}_z - \beta(e^{j(\omega\Delta t)} + 1)\tilde{E}_z = 0 \qquad (A.3)$$

$$\left(e^{j(\omega\Delta t)} - A\right)\tilde{E}_x + Be^{j\left(\omega\frac{\Delta t}{2}\right)}\left[\left(\frac{e^{j\left(k_y\frac{\Delta y}{2}\right)} - e^{-j\left(k_y\frac{\Delta y}{2}\right)}}{\Delta y}\right)\widetilde{H}_z - \left(\frac{e^{j\left(k_z\frac{\Delta z}{2}\right)} - e^{-j\left(k_z\frac{\Delta z}{2}\right)}}{\Delta z}\right)\widetilde{H}_y\right] - C\,\check{J}_x = 0 \qquad (A.4)$$

$$\left(e^{j(\omega\Delta t)} - A\right)\tilde{E}_y + Be^{j\left(\omega\frac{\Delta t}{2}\right)}\left[\left(\frac{e^{j\left(k_z\frac{\Delta z}{2}\right)} - e^{j\left(k_z\frac{\Delta z}{2}\right)}}{\Delta z}\right)\widetilde{H}_x - \left(\frac{e^{j\left(k_x\frac{\Delta x}{2}\right)} - e^{-j\left(k_x\frac{\Delta x}{2}\right)}}{\Delta x}\right)\widetilde{H}_z\right] - C\,\check{J}_y = 0 \qquad (A.5)$$

$$\left(e^{j(\omega\Delta t)}-A\right)\tilde{E}_z + Be^{j\left(\omega\frac{\Delta t}{2}\right)}\begin{bmatrix}\left(\frac{e^{j\left(k_x\frac{\Delta x}{2}\right)}-e^{-j\left(k_x\frac{\Delta x}{2}\right)}}{\Delta x}\right)\tilde{H}_y \\ -\left(\frac{e^{j\left(k_y\frac{\Delta y}{2}\right)}-e^{-j\left(k_y\frac{\Delta y}{2}\right)}}{\Delta y}\right)\tilde{H}_x\end{bmatrix} - C\,\check{J}_z = 0 \qquad (A.6)$$

$$\left(e^{j\left(\omega\frac{\Delta t}{2}\right)}-e^{-j\left(\omega\frac{\Delta t}{2}\right)}\right)\tilde{H}_x + \frac{\Delta t}{\mu}\begin{bmatrix}\left(\frac{e^{j\left(k_y\frac{\Delta y}{2}\right)}-e^{-j\left(k_y\frac{\Delta y}{2}\right)}}{\Delta y}\right)\tilde{E}_z \\ -\left(\frac{e^{j\left(k_z\frac{\Delta z}{2}\right)}-e^{j\left(k_z\frac{\Delta z}{2}\right)}}{\Delta z}\right)\tilde{E}_y\end{bmatrix} = 0 \quad (A.7)$$

$$\left(e^{j\left(\omega\frac{\Delta t}{2}\right)}-e^{-j\left(\omega\frac{\Delta t}{2}\right)}\right)\tilde{H}_y + \frac{\Delta t}{\mu}\begin{bmatrix}\left(\frac{e^{j\left(k_z\frac{\Delta z}{2}\right)}-e^{j\left(k_z\frac{\Delta z}{2}\right)}}{\Delta z}\right)\tilde{E}_x \\ -\left(\frac{e^{j\left(k_x\frac{\Delta x}{2}\right)}-e^{-j\left(k_x\frac{\Delta x}{2}\right)}}{\Delta x}\right)\tilde{E}_z\end{bmatrix} = 0 \quad (A.8)$$

$$\left(e^{j\left(\omega\frac{\Delta t}{2}\right)}-e^{-j\left(\omega\frac{\Delta t}{2}\right)}\right)\tilde{H}_z + \frac{\Delta t}{\mu}\begin{bmatrix}\left(\frac{e^{j\left(k_x\frac{\Delta x}{2}\right)}-e^{-j\left(k_x\frac{\Delta x}{2}\right)}}{\Delta x}\right)\tilde{E}_y \\ -\left(\frac{e^{j\left(k_y\frac{\Delta y}{2}\right)}-e^{-j\left(k_y\frac{\Delta y}{2}\right)}}{\Delta y}\right)\tilde{E}_x\end{bmatrix} = 0 \quad (A.9)$$

We reach to this system of equation following by the matrix to construct $\bar{A}X = 0$:

$$
\begin{cases}
\acute{a}\tilde{J}_x - \acute{b}\tilde{E}_x = 0 & (a.1)\\
\acute{a}\tilde{J}_y - \acute{b}\tilde{E}_y = 0 & (a.2)\\
\acute{a}\tilde{J}_z - \acute{b}\tilde{E}_z = 0 & (a.3)\\
\acute{c}\tilde{E}_x + \acute{d}\tilde{H}_z - \acute{e}\tilde{H}_y - C\,\check{J}_x = 0 & (a.4)\\
\acute{c}\tilde{E}_y + \acute{e}\tilde{H}_x - \acute{f}\tilde{H}_z - C\,\check{J}_y = 0 & (a.5)\\
\acute{c}\tilde{E}_z + \acute{f}\tilde{H}_y - \acute{d}\tilde{H}_x - C\,\check{J}_z = 0 & (a.6)\\
\acute{g}\tilde{H}_x + \acute{\acute{d}}\tilde{E}_z - \acute{\acute{e}}\tilde{E}_y = 0 & (a.7)\\
\acute{g}\tilde{H}_y + \acute{\acute{e}}\tilde{E}_x - \acute{\acute{f}}\tilde{E}_z = 0 & (a.8)\\
\acute{g}\tilde{H}_z + \acute{\acute{f}}\tilde{E}_y - \acute{\acute{d}}\tilde{E}_x = 0 & (a.9)
\end{cases}
\qquad (A.10)
$$

$$
\bar{A}X = \begin{bmatrix}
+\acute{a} & 0 & 0 & -\acute{b} & 0 & 0 & 0 & 0 & 0\\
0 & +\acute{a} & 0 & 0 & -\acute{b} & 0 & 0 & 0 & 0\\
0 & 0 & +\acute{a} & 0 & 0 & -\acute{b} & 0 & 0 & 0\\
-C & 0 & 0 & \acute{c} & 0 & 0 & 0 & -\acute{e} & \acute{d}\\
0 & -C & 0 & 0 & \acute{c} & 0 & \acute{e} & 0 & -\acute{f}\\
0 & 0 & -C & 0 & 0 & \acute{c} & -\acute{d} & \acute{f} & 0\\
0 & 0 & 0 & 0 & -\acute{\acute{e}} & +\acute{\acute{d}} & \acute{g} & 0 & 0\\
0 & 0 & 0 & +\acute{\acute{e}} & 0 & -\acute{\acute{f}} & 0 & \acute{g} & 0\\
0 & 0 & 0 & -\acute{\acute{d}} & +\acute{\acute{f}} & 0 & 0 & 0 & \acute{g}
\end{bmatrix}
\begin{bmatrix}
\tilde{J}_x\\ \tilde{J}_y\\ \tilde{J}_z\\ \tilde{E}_x\\ \tilde{E}_y\\ \tilde{E}_z\\ \tilde{H}_x\\ \tilde{H}_y\\ \tilde{H}_z
\end{bmatrix} = 0 \qquad (A.11)
$$

The elements of Matrix A is as follows:

$$\acute{a} = e^{j(\omega\Delta t)} - \alpha, \qquad \acute{b} = \beta(e^{j(\omega\Delta t)} + 1), \qquad \acute{c} = e^{j(\omega\Delta t)} - A \qquad (A.12)$$

$$d = \frac{e^{j\left(k_y\frac{\Delta y}{2}\right)} - e^{-j\left(k_y\frac{\Delta y}{2}\right)}}{\Delta y} = \frac{2jsin(k_y\frac{\Delta y}{2})}{\Delta y} \rightarrow \quad \acute{d} = Be^{j\left(\omega\frac{\Delta t}{2}\right)}d \quad (A.13)$$

$$e = \frac{e^{j\left(k_z\frac{\Delta z}{2}\right)} - e^{-j\left(k_z\frac{\Delta z}{2}\right)}}{\Delta z} = \frac{2jsin(k_z\frac{\Delta z}{2})}{\Delta z} \rightarrow \quad \acute{e} = Be^{j\left(\omega\frac{\Delta t}{2}\right)}e \quad (A.14)$$

$$f = \frac{e^{j\left(k_x\frac{\Delta x}{2}\right)} - e^{-j\left(k_x\frac{\Delta x}{2}\right)}}{\Delta x} = \frac{2jsin(k_x\frac{\Delta x}{2})}{\Delta x} \rightarrow \quad \acute{f} = Be^{j\left(\omega\frac{\Delta t}{2}\right)}f \quad (A.15)$$

$$\acute{g} = \left(e^{j\left(\omega\frac{\Delta t}{2}\right)} - e^{-j\left(\omega\frac{\Delta t}{2}\right)}\right) = 2j\,sin\left(\omega\frac{\Delta t}{2}\right) \qquad (A.16)$$

$$\acute{\acute{d}} = \frac{\Delta t}{\mu}d, \qquad \acute{\acute{e}} = \frac{\Delta t}{\mu}e, \qquad \acute{\acute{f}} = \frac{\Delta t}{\mu}f \qquad (A.17)$$

In order to calculate the dispersion relation we need to set $Det(X)$ to zero:

$$Det(X) = \acute{g}(\acute{a}\acute{c} + \acute{b}C)(-\acute{b}Cg - \acute{a}\acute{c}g - \acute{a}\acute{e}\acute{\acute{e}} - \acute{a}\acute{d}\acute{\acute{d}} + \acute{a}\acute{f}\acute{\acute{f}})^2 \qquad (A.18)$$

By substituting the variables, Dispersion relation is:

$$\left(e^{j\omega\Delta t} - \alpha\right)\left(-e^{j\omega\Delta t} - A\right)\left(4sin^2\left(\frac{\omega\Delta t}{2}\right)\right) - 4\frac{\Delta t^2 c^2}{\Delta x^2}sin^2\left(\frac{k_x\Delta x}{2}\right) - 4\frac{\Delta t^2 c^2}{\Delta y^2}sin^2\left(\frac{k_y\Delta y}{2}\right)$$
$$- 4\frac{\Delta t^2 c^2}{\Delta z^2}sin^2\left(\frac{k_z\Delta z}{2}\right) + 4j\beta\frac{\Delta t}{\varepsilon}cos^2\left(\frac{\omega\Delta t}{2}\right)sin\left(\frac{\Delta t}{2}\right) = 0, \qquad (A.19)$$

Appendix B

Derivation of Mass and Stiffness Matrices of VWE with Graphene

As mentioned before, Yee's FDTD is equivalent to mass-lumped FETD on a mesh composed of blocks [44]. By expanding E field in Whitney 1-form for edge elements $e = \{i, j\}$ and B field in Whitney 2-form for face elements $f = \{i, j, k\}$, the shape functions are:

$$w_e = w_i \nabla w_j - w_j \nabla w_i \qquad (B.1)$$

$$w_f = 2\left(w_i \nabla w_j \times \nabla w_k + w_j \nabla w_k \times \nabla w_i + w_k \nabla w_i \times \nabla w_j\right) \qquad (B.2)$$

The edge element preserve tangential continuity while face element maintains the normal continuity across the boundaries.

In the case of 1D, consider a uniform axes of edge length ΔL, with graphene at second edge as shown in Fig. B.1:

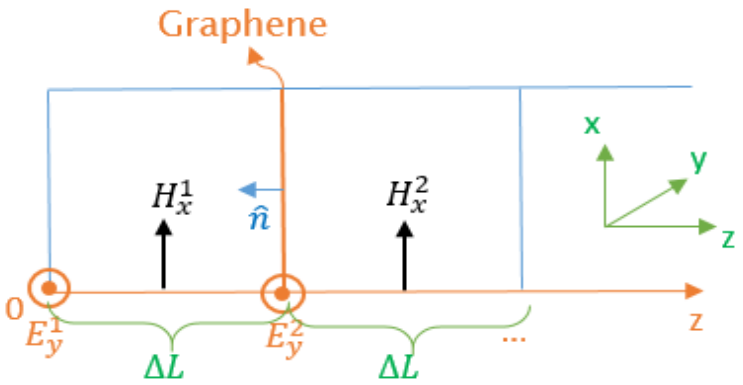

Fig.B.1. 1D scheme for Whitney edge and face element

It is apparent that Whitney functions can be introduce as follow:

$$W_1^{(1)} = \left(\frac{\Delta L - Z}{\Delta L}\right)\hat{y},\ \ W_2^{(1)} = \left(\frac{Z}{\Delta L}\right)\hat{y} \quad and\ W^{(2)} = (1)\hat{x} \qquad (B.3)$$

Applying Trapezoidal rule on equation (3.5), (3.7) and (B.3) we will have:

$$T_{11} = \int \epsilon W_1^{(1)}.W_1^{(1)}\, dl = \epsilon \int \left(\frac{\Delta L - Z}{\Delta L}\right)^2 \hat{y}.\hat{y}\, dz = \epsilon\frac{\Delta L}{2}\,(1+0) = \epsilon\frac{\Delta L}{2} \quad (B.4)$$

$$T_{12} = T_{21} = \int \epsilon W_1^{(1)}.W_2^{(1)}\, dl = \epsilon \int \left(\frac{\Delta L - Z}{\Delta L}\right)\left(\frac{Z}{\Delta L}\right)\hat{y}.\hat{y}\, dl = \epsilon\frac{\Delta L}{2}\,(0+0) = 0 \quad (B.5)$$

$$T_{22} = \int \epsilon W_1^{(1)}.W_1^{(1)}\, dl = \epsilon \int \left(\frac{Z}{\Delta L}\right)^2 \hat{y}.\hat{y}\, dl = \epsilon\frac{\Delta L}{2}\,(1+0) = \epsilon\frac{\Delta L}{2} \qquad (B.6)$$

$$T_f = \int \mu^{-1} 1.1\, dl = \mu^{-1}\Delta L \qquad (B.7)$$

$$T_{e1} = \epsilon\begin{bmatrix}\frac{\Delta L}{2} & 0\\ 0 & \frac{\Delta L}{2}\end{bmatrix},\ \ T_{e2} = \epsilon\begin{bmatrix}\frac{\Delta L}{2} & 0\\ 0 & \frac{\Delta L}{2}\end{bmatrix}, \ldots \quad (B.8)$$

Assembling all the elements results in the total mass matrix:

$$T = \epsilon\begin{bmatrix}\frac{\Delta L}{2} & 0 & 0 & 0\\ 0 & \Delta L & 0 & 0\\ 0 & 0 & \Delta L & 0\\ 0 & 0 & 0 & \frac{\Delta L}{2}\end{bmatrix} \qquad (B.9)$$

It is obvious that apart from boundary edges we can approximate $T = \epsilon\Delta L$. Applying Trapezoidal rule on equation (4.4) which concerns the graphene layer, gives:

$$Q_{g_{11}} = \int \left(\hat{n} \times \left(\frac{\Delta L - Z}{\Delta L}\right)\hat{y}\right).\left(\hat{n} \times \left(\frac{\Delta L - Z}{\Delta L}\right)\hat{y}\right).dl, \quad \hat{n} \times \hat{y} = \hat{x} \qquad (B.10)$$

$$Q_{g_{11}} = \int \left(\frac{\Delta L - Z}{\Delta L}\right)^2 \hat{x}.\hat{x}\ dz = 0\ \ (there\ is\ no\ graphene\ at\ 1st\ edge) \qquad (B.11)$$

$$Q_{g_{22}} = \int \left(\hat{n} \times \left(\frac{Z}{\Delta L}\right)\hat{y}\right).\left(\hat{n} \times \left(\frac{Z}{\Delta L}\right)\hat{y}\right) = \int \left(\frac{Z}{\Delta L}\right)^2 \hat{x}.\hat{x}\, dz = 1 \qquad (B.12)$$

$$Q_{g_{12}} = Q_{g_{12}} = \int \left(\hat{n} \times \left(\frac{\Delta L - Z}{\Delta L}\right)\hat{y}\right).\left(\hat{n} \times \left(\frac{Z}{\Delta L}\right)\hat{y}\right) = 0 \qquad (B.13)$$

As we can see, matrix Q= $\begin{bmatrix} 0 & 0 \\ 0 & 1 \end{bmatrix}$ is a diagonal matrix with nonzero values only on the edges containing graphene. C is the curl matrix which is a linear combination of the face elements and their related edges:

$$C = \frac{1}{\Delta L}\begin{bmatrix} 1 & -1 & 0 \\ 0 & 1 & -1 \end{bmatrix} \qquad (B.14)$$

In the case of 2D, four elements with the length of the edges ΔL is considered here;

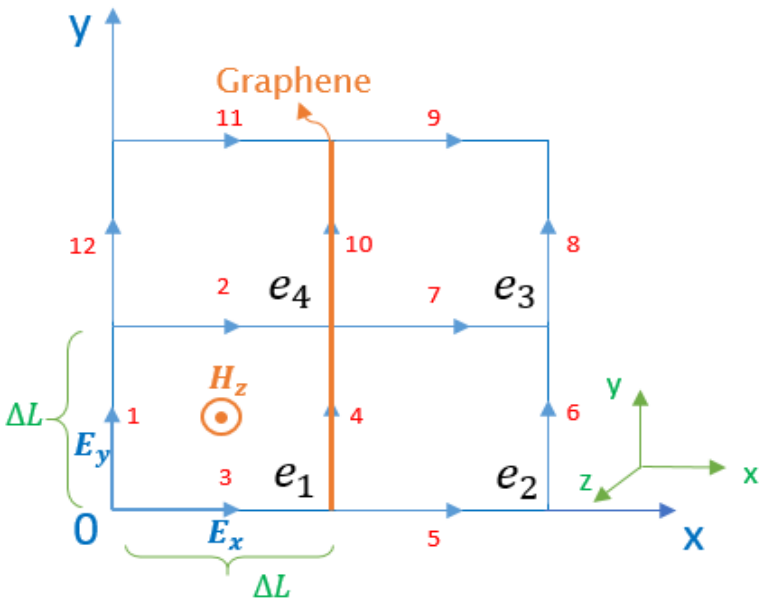

Fig.B.2. 2D scheme for Whitney edge and face element.

In this case, shape functions will be as follow:

$$W_1^{(1)} = \left(\frac{\Delta L - x}{\Delta L}\right)\hat{y} \qquad W_2^{(1)} = \left(\frac{y}{\Delta L}\right)\hat{x} \qquad W_3^{(1)} = \left(\frac{\Delta L - y}{\Delta L}\right)\hat{x}$$

$$W_4^{(1)} = \left(\frac{x}{\Delta L}\right)\hat{y} \qquad W^{(2)} = \left(\frac{\Delta L - z}{\Delta L}\right)\hat{z} \qquad (B.15)$$

Again by applying Trapezoid rule of equation (3.5),(3.7) for element 1, gives:

$$T_{11} = \epsilon \int \left(\frac{\Delta L - x}{\Delta L}\right)\hat{y}.\left(\frac{\Delta L - x}{\Delta L}\right)\hat{y}.dy = \epsilon\frac{\Delta L^2}{4}\,(1+0+1+0) = \epsilon\frac{\Delta L^2}{2} \quad (B.16)$$

$$T_{11} = T_{22} = T_{33} = T_{44} \quad (B.17)$$

$$T_{12} = T_{21} = \int \left(\frac{\Delta L - x}{\Delta L}\right)\hat{y}.\left(\frac{y}{\Delta L}\right)\hat{x}\,dl = 0 \quad (B.18)$$

$$T_{13} = T_{31} = \int \left(\frac{\Delta L - x}{\Delta L}\right)\hat{y}.\left(\frac{\Delta L - y}{\Delta L}\right)\hat{x}\,dl = 0 \quad (B.19)$$

$$T_{14} = T_{41} = \int \left(\frac{\Delta L - x}{\Delta L}\right)\hat{y}.\left(\frac{x}{\Delta L}\right)\hat{y}\,dl = 0 \quad (B.20)$$

$$T_{23} = T_{32} = \int \left(\frac{\Delta L - y}{\Delta L}\right)\hat{x}.\left(\frac{y}{\Delta L}\right)\hat{x}\,dl = 0 \quad (B.21)$$

$$T_{f1} = \int \mu^{-1}\left(\frac{\Delta L - z}{\Delta L}\right)\hat{z}.\left(\frac{\Delta L - z}{\Delta L}\right)\hat{z}\,dl = \mu^{-1}\Delta L^2 \quad (B.22)$$

$$T_{f1} = T_{f2} = T_{f3} = T_{f4} \quad (B.23)$$

$$T_{e1} = T_{e2} = T_{e3} = T_{e4} = \epsilon\begin{bmatrix} \frac{\Delta L^2}{2} & 0 & 0 & 0 \\ 0 & \frac{\Delta L^2}{2} & 0 & 0 \\ 0 & 0 & \frac{\Delta L^2}{2} & 0 \\ 0 & 0 & 0 & \frac{\Delta L}{2} \end{bmatrix} \quad (B.24)$$

After assembly we will have:

$$T_{12\times 12} = \epsilon\begin{bmatrix} \frac{\Delta L^2}{2} & \cdots & 0 \\ \vdots & \Delta L^2 & \vdots \\ 0 & \cdots & \ddots \end{bmatrix} \quad (B.25)$$

$$T_f = \mu^{-1}\begin{bmatrix} \Delta L^2 & 0 \\ 0 & \Delta L^2 \end{bmatrix} \quad (B.26)$$

For equation (4.4), we will have:

$$Q_{g_{11}} = \int \left(n \times \left(\frac{\Delta L - x}{\Delta L}\right)\hat{y}\right).\left(n \times \left(\frac{\Delta L - x}{\Delta L}\right)\hat{y}\right).dl = 0 \quad (B.27)$$

$$Q_{g_{11}} = Q_{g_{22}} = Q_{g_{33}} = 0 \tag{B.28}$$

$$Q_{g_{44}} = \int \left(n \times \left(\frac{x}{\Delta L}\right)\hat{y}\right).\left(n \times \left(\frac{x}{\Delta L}\right)\hat{y}\right).dl = \Delta L \tag{B.29}$$

$$Q_{g_{14}} = \int \left(n \times \left(\frac{\Delta L - x}{\Delta L}\right)\hat{y}\right).\left(n \times \left(\frac{x}{\Delta L}\right)\hat{y}\right).dl = 0, \;\; n \times \hat{y} = -i \times j = -k \tag{B.30}$$

$$\begin{gathered} Q_{g_{14}} = Q_{g_{41}} = 0, \quad Q_{g_{24}} = Q_{g_{42}} = 0, \quad Q_{g_{34}} = Q_{g_{43}} = 0, \\ Q_{g_{32}} = Q_{g_{23}} = 0\,, \quad Q_{g_{31}} = Q_{g_{13}} = 0, \quad Q_{g_{21}} = Q_{g_{12}} = 0 \end{gathered} \tag{B.31}$$

$$Q_{12\times 12} = \begin{bmatrix} 0 & \cdots & 0 & & 0 & \cdots & 0 \\ \vdots & \ddots & \vdots & \dots & \vdots & \ddots & \vdots \\ 0 & \cdots & 2\Delta L & & 0 & \cdots & 0 \\ 0 & \cdots & 0 & & 0 & \cdots & 0 \\ \vdots & \ddots & \vdots & \dots & \vdots & \ddots & \vdots \\ 0 & \cdots & 0 & & 0 & \cdots & 0 \end{bmatrix} \tag{B.32}$$

which is diagonal matrix with diagonal elements which does not contain graphene are equal to zero.